

Fig. 1A

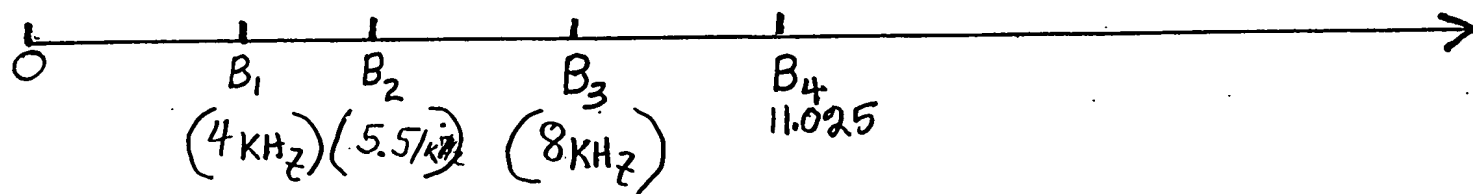


Fig. 1B

FFT-based Scalable and Embedded Codec Architecture — Encoder with M Octave Bands

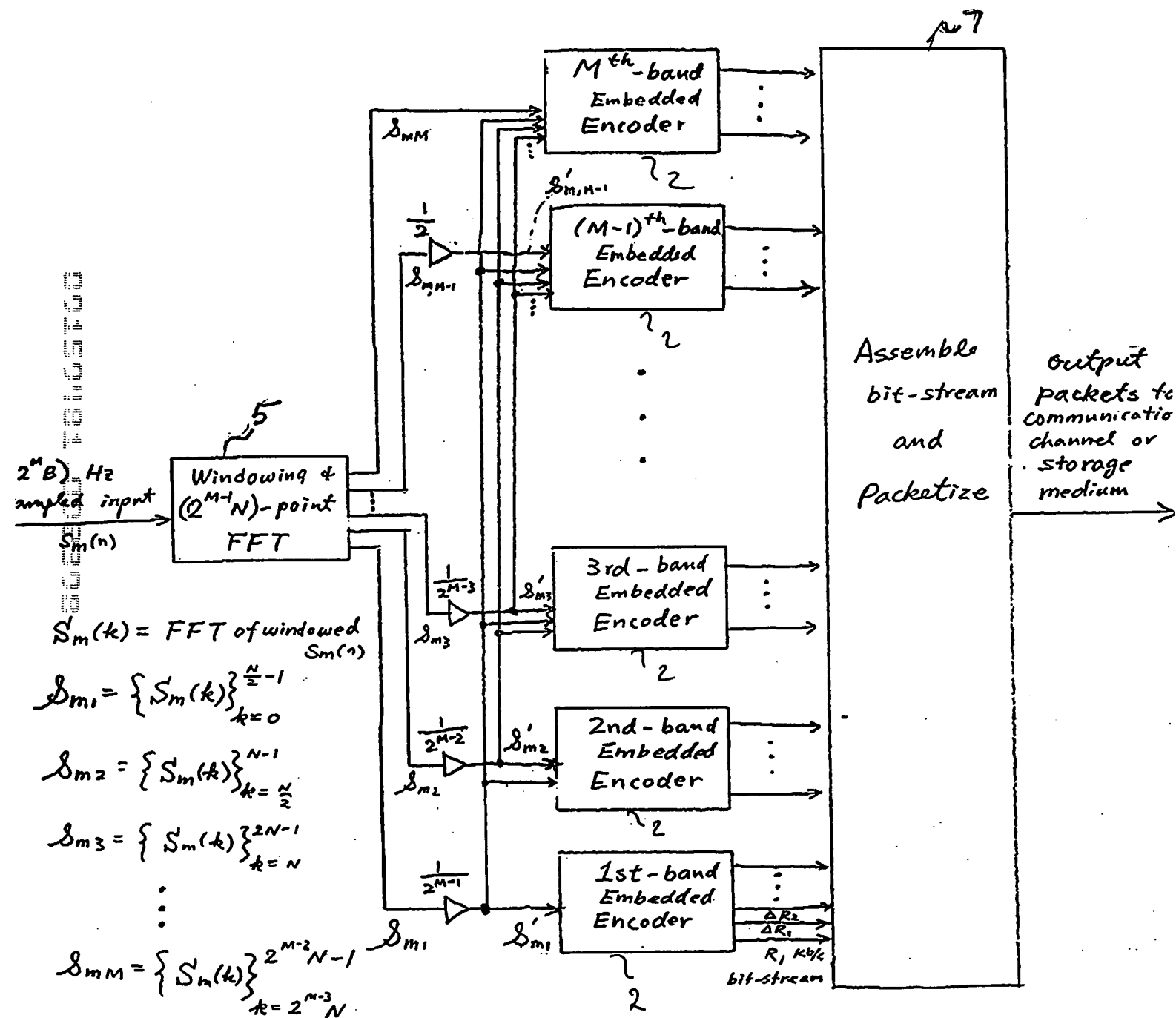


Fig. 2A

FFT-based Scalable and Embedded Codec Architecture — Decoder with M_1 Octave Bands ($1 \leq M_1 \leq M$)

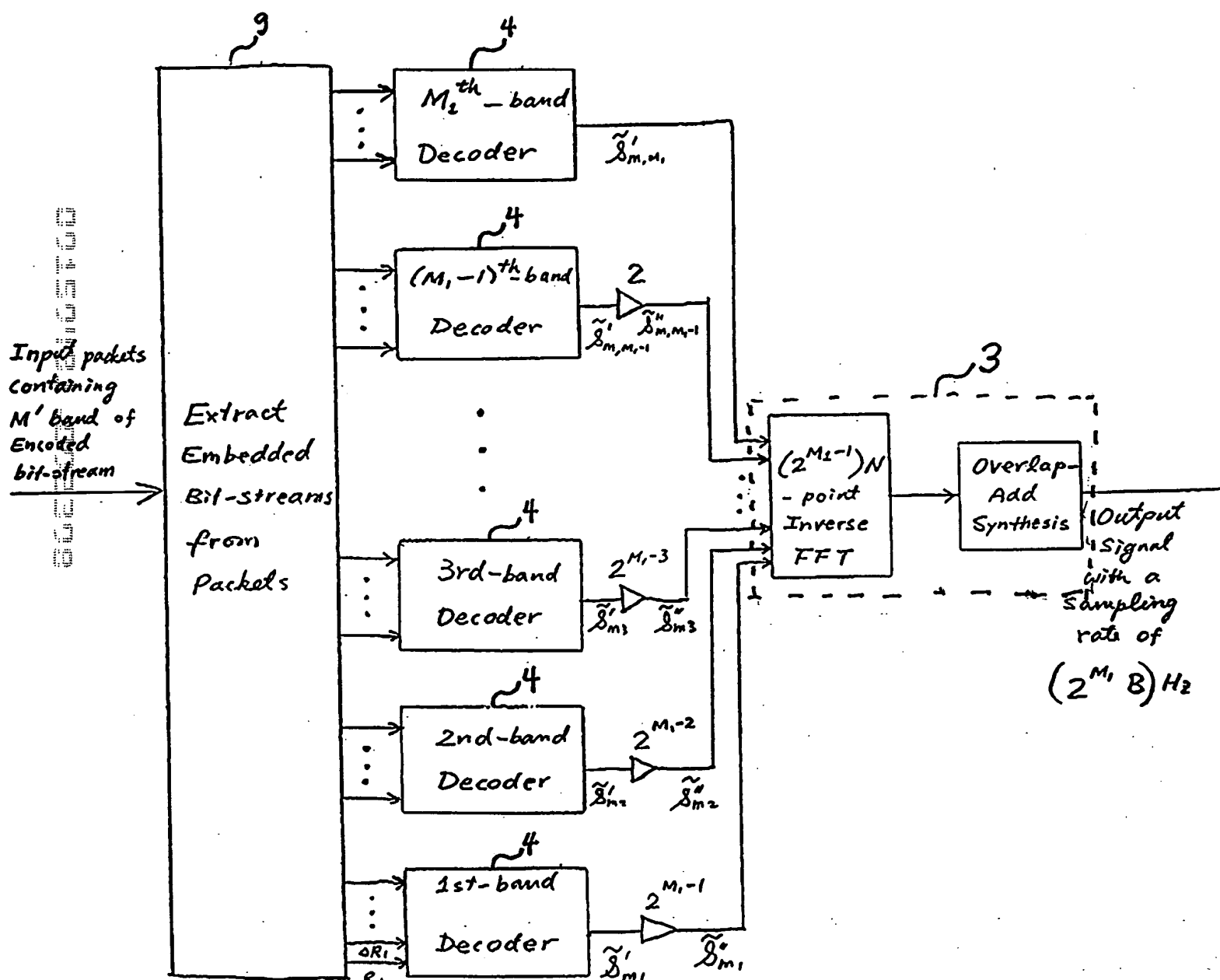


Fig. 2B

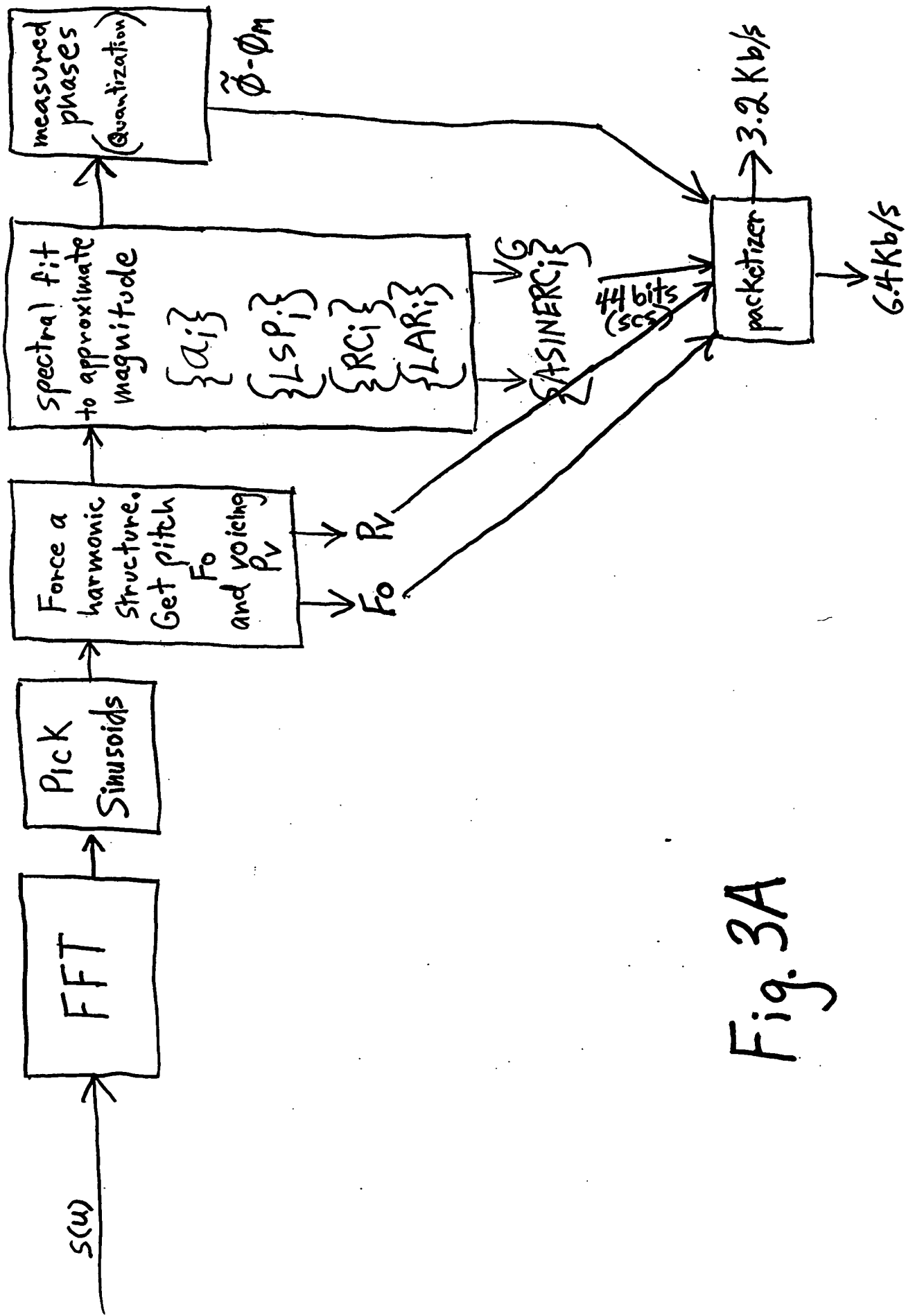
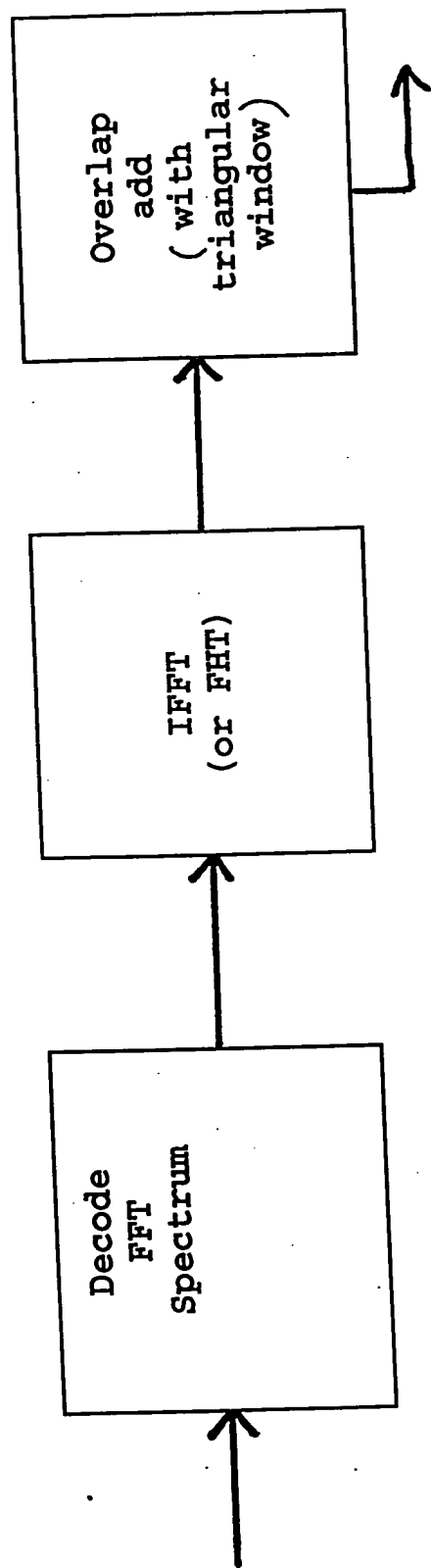


Fig. 3A



Decoder: Synthesis every M ms.

Fig. 3B

Bit Stream Division

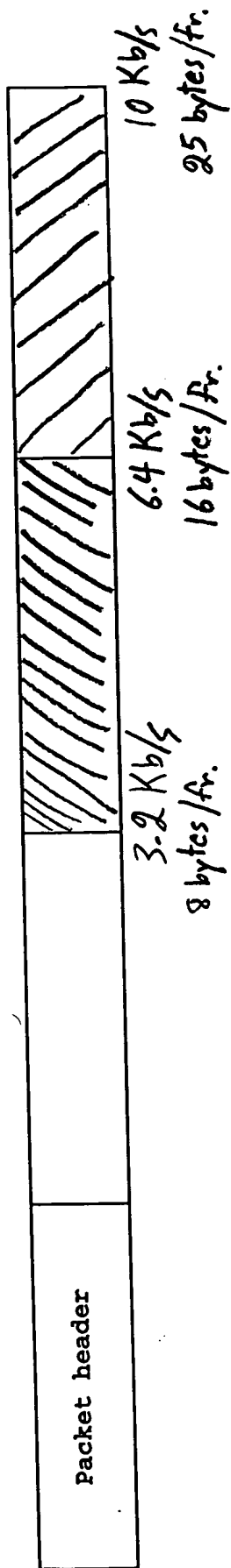


Fig. 4A

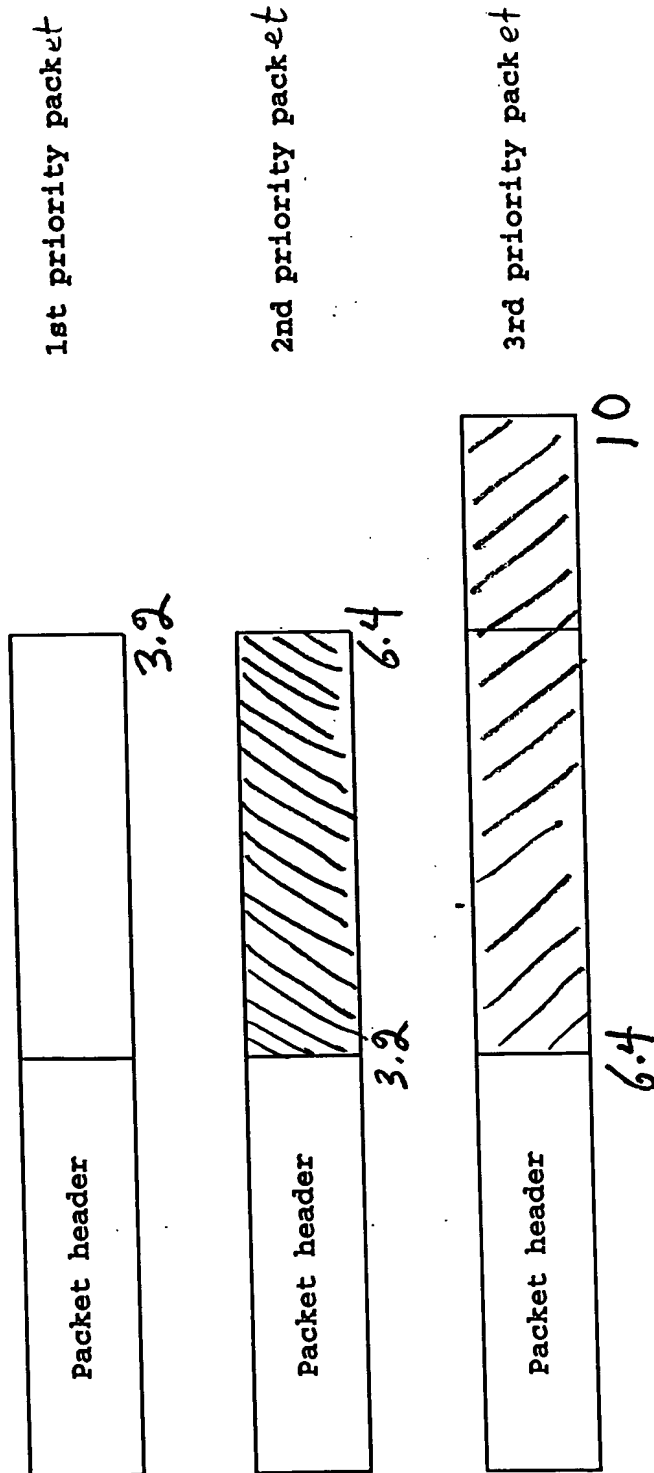
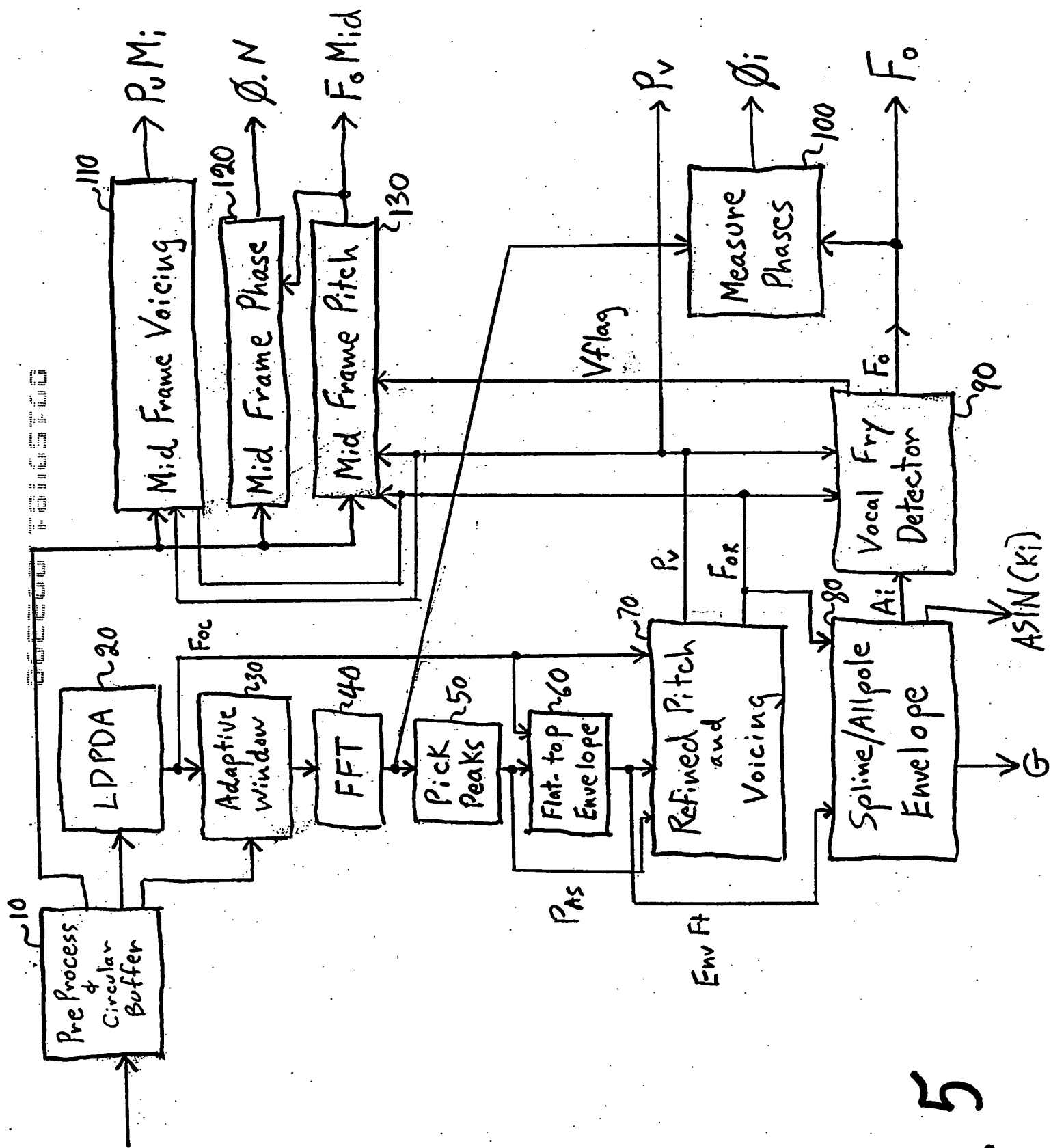


Fig. 4B



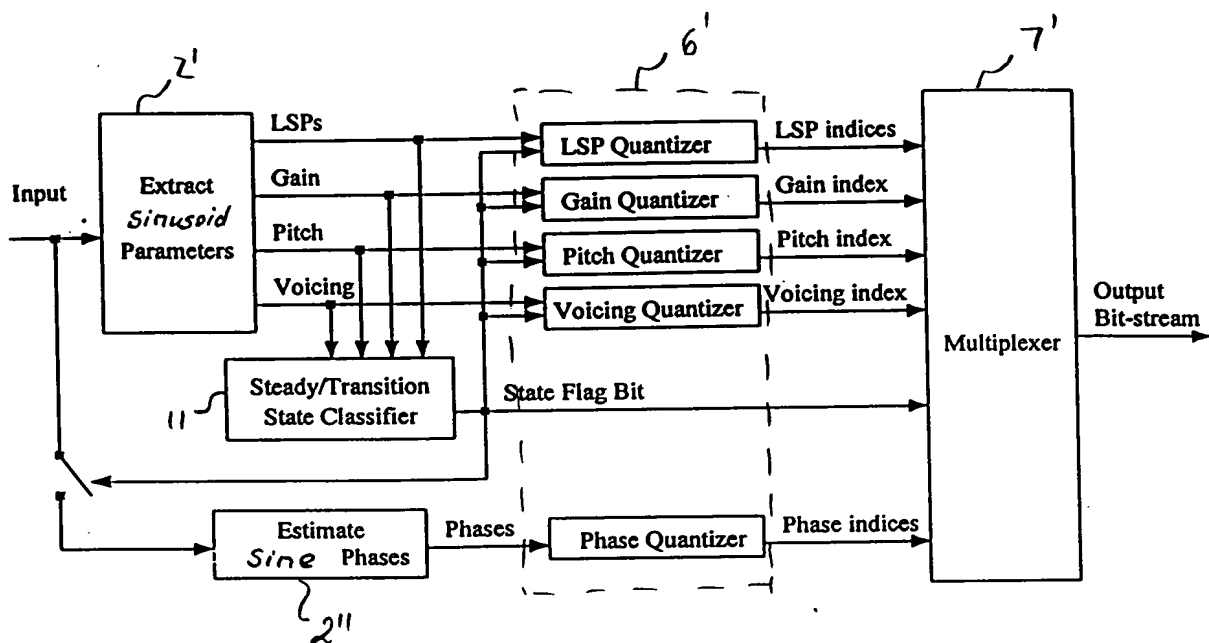


Fig 5A

SC3-6-10 SINE WAVE SINE WAVE SINE WAVE SPEECH SYNTHESIZER

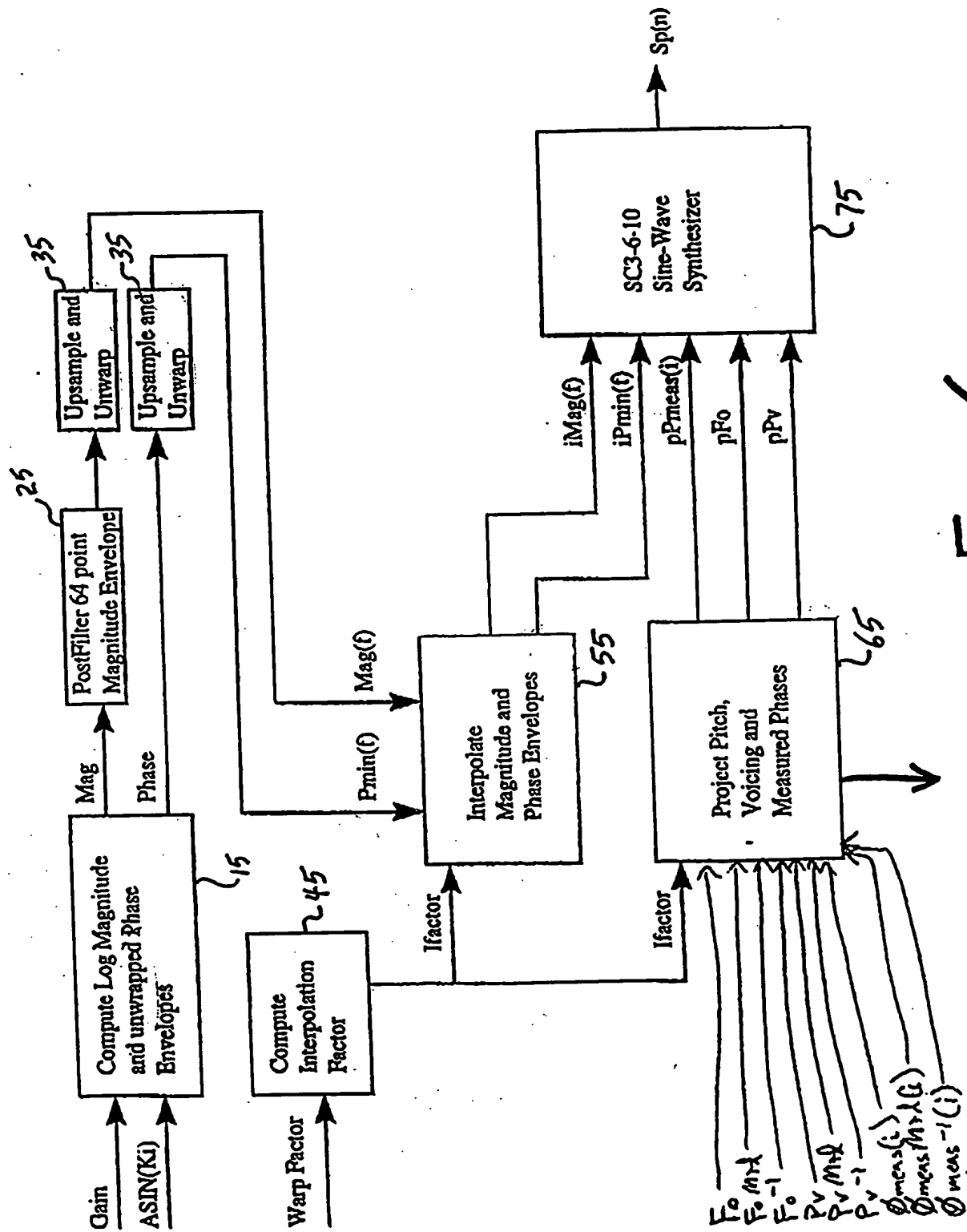


Fig. 6

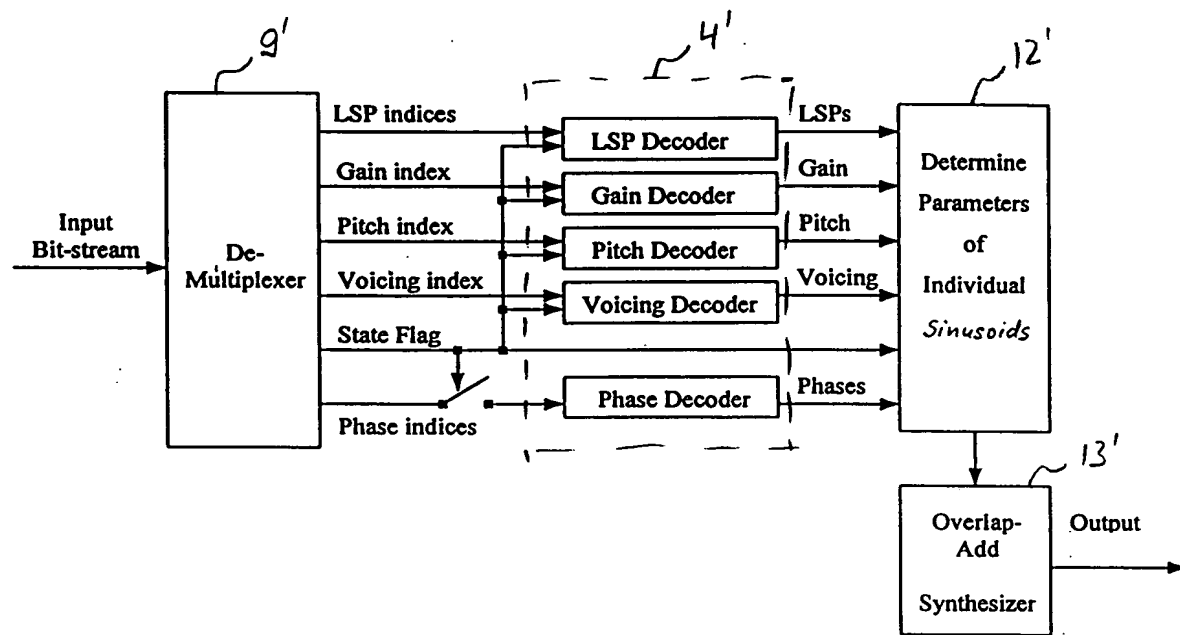


Fig. 6A

SC3-6-10 SINE WAVE SYNTHESIZER

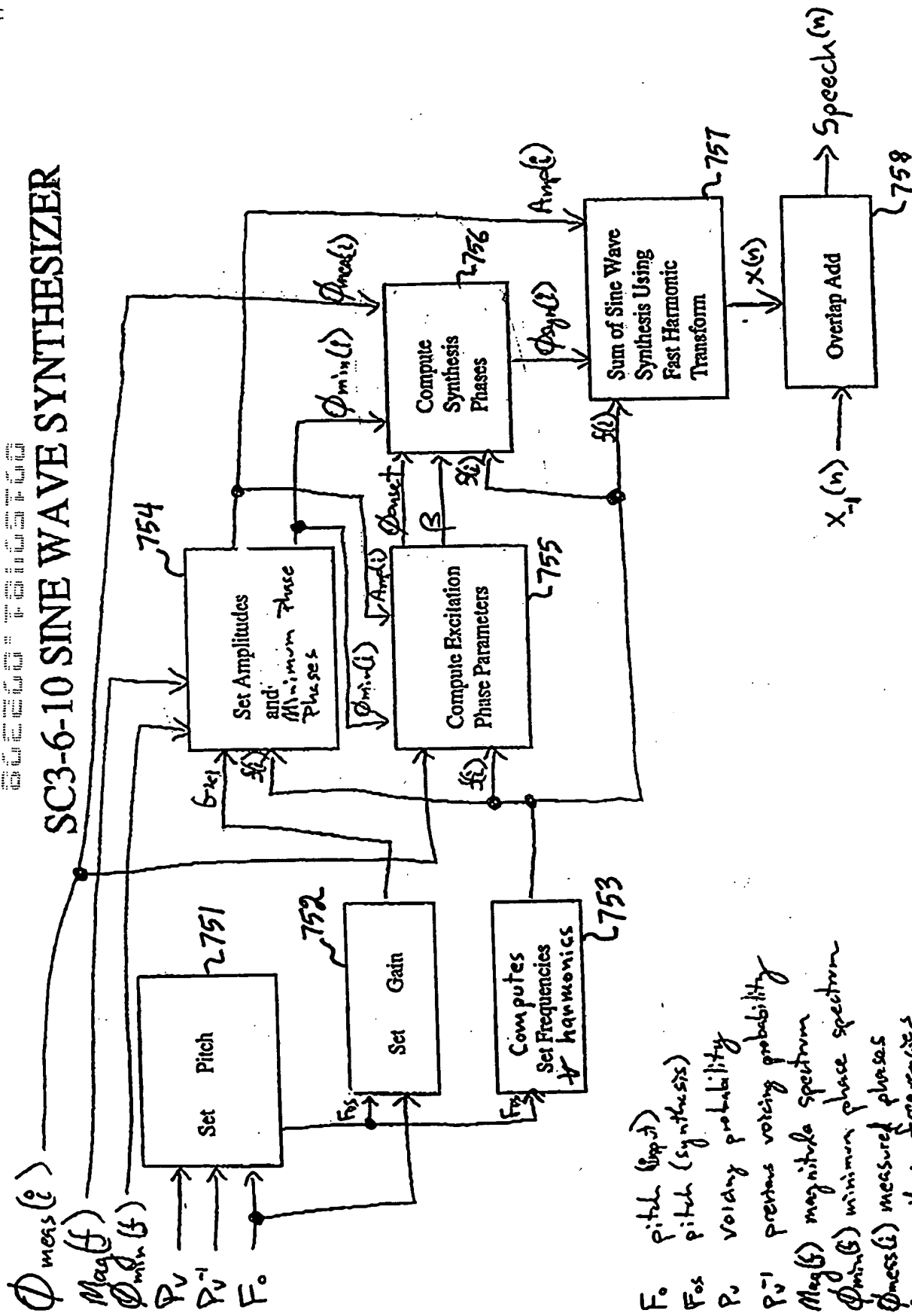


Fig. 7

- F_0 pitch (input)
- F_{0s} pitch (synthesis)
- P_v voicing probability
- P_v^{-1} previous voicing probability
- $Mag(f)$ magnitude spectrum
- $\Phi_{min}(f)$ minimum phase spectrum
- $\Phi_{meas}(i)$ measured phases
- f_i synthesis frequencies
- $Ampl(i)$ synthesis amplitudes
- $\Phi_{syn}(i)$ synthesis phases
- $\Phi_{min}(i)$ minimum phases at f_i

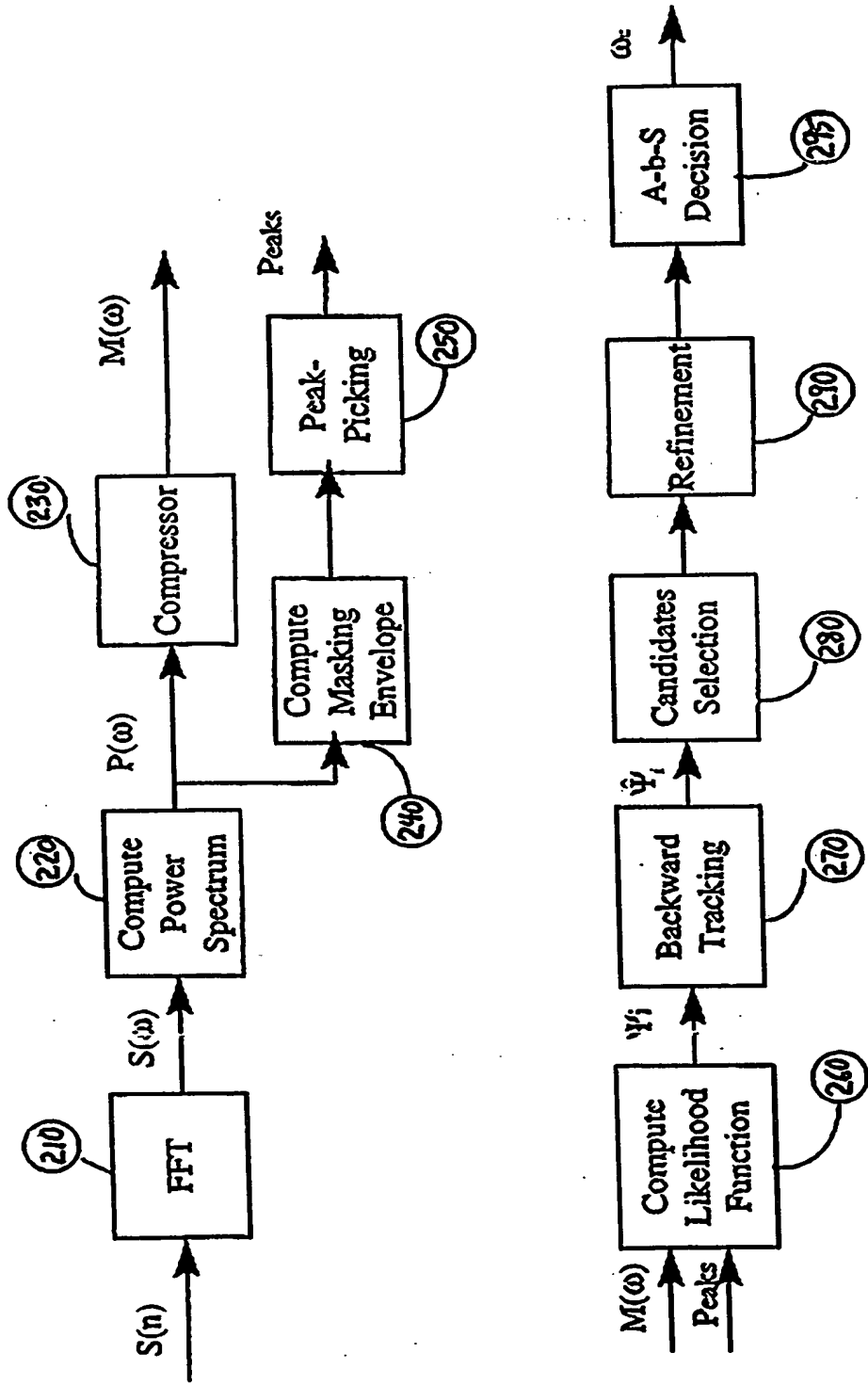


Fig. 8

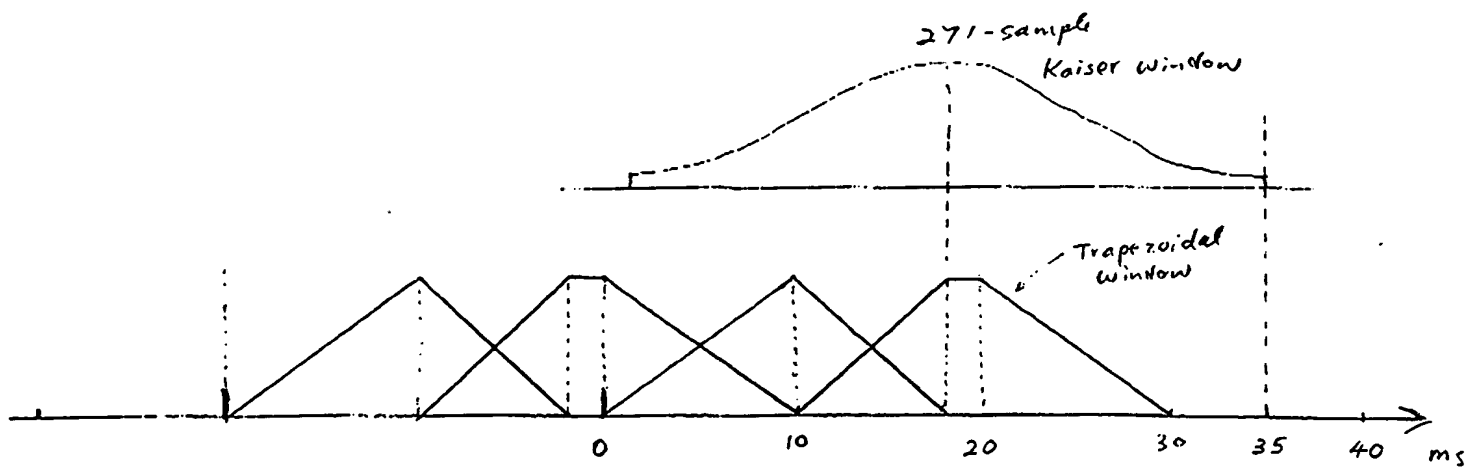


Fig. 8. A

56666-10100000

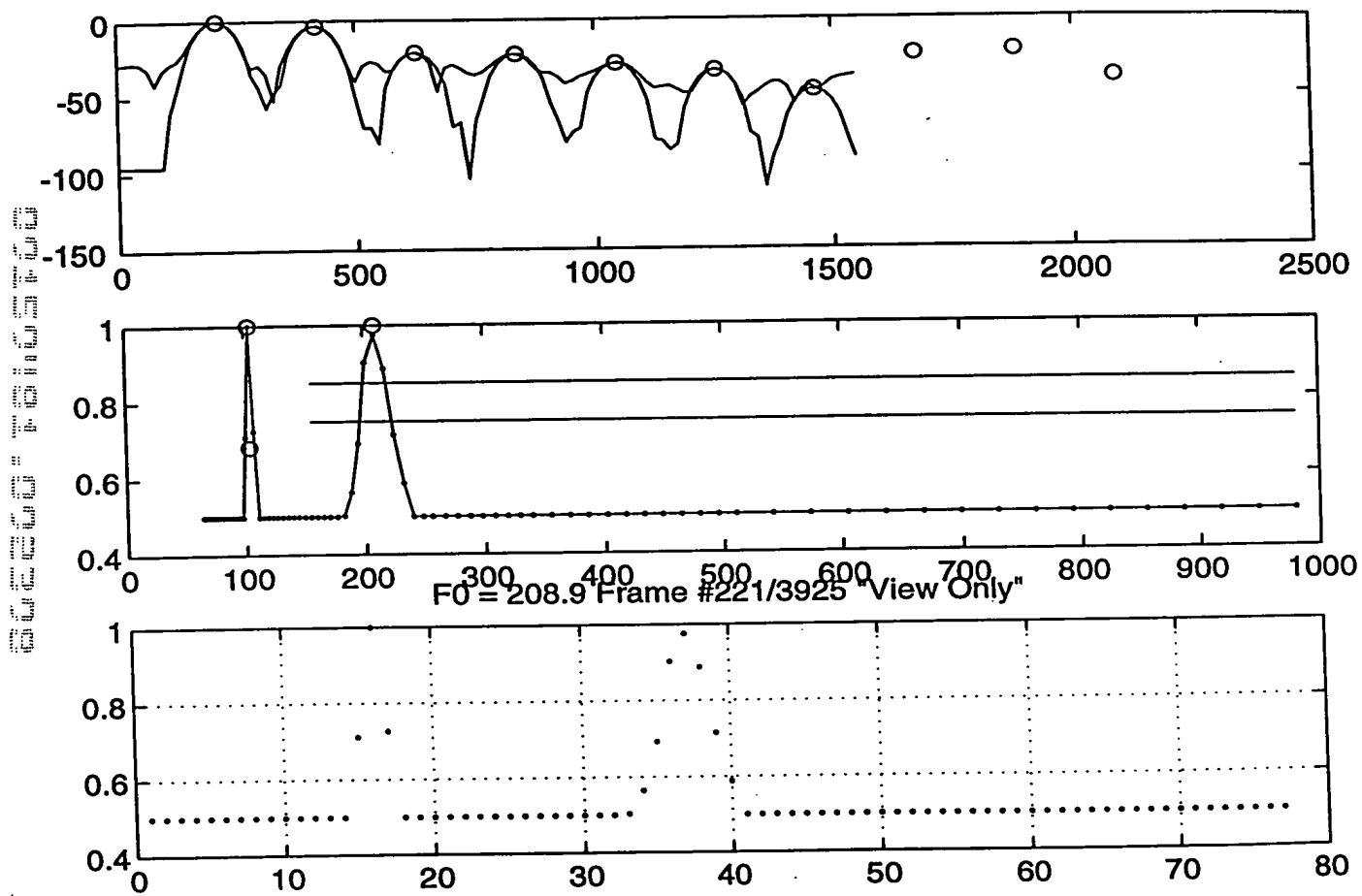


Fig. 9A

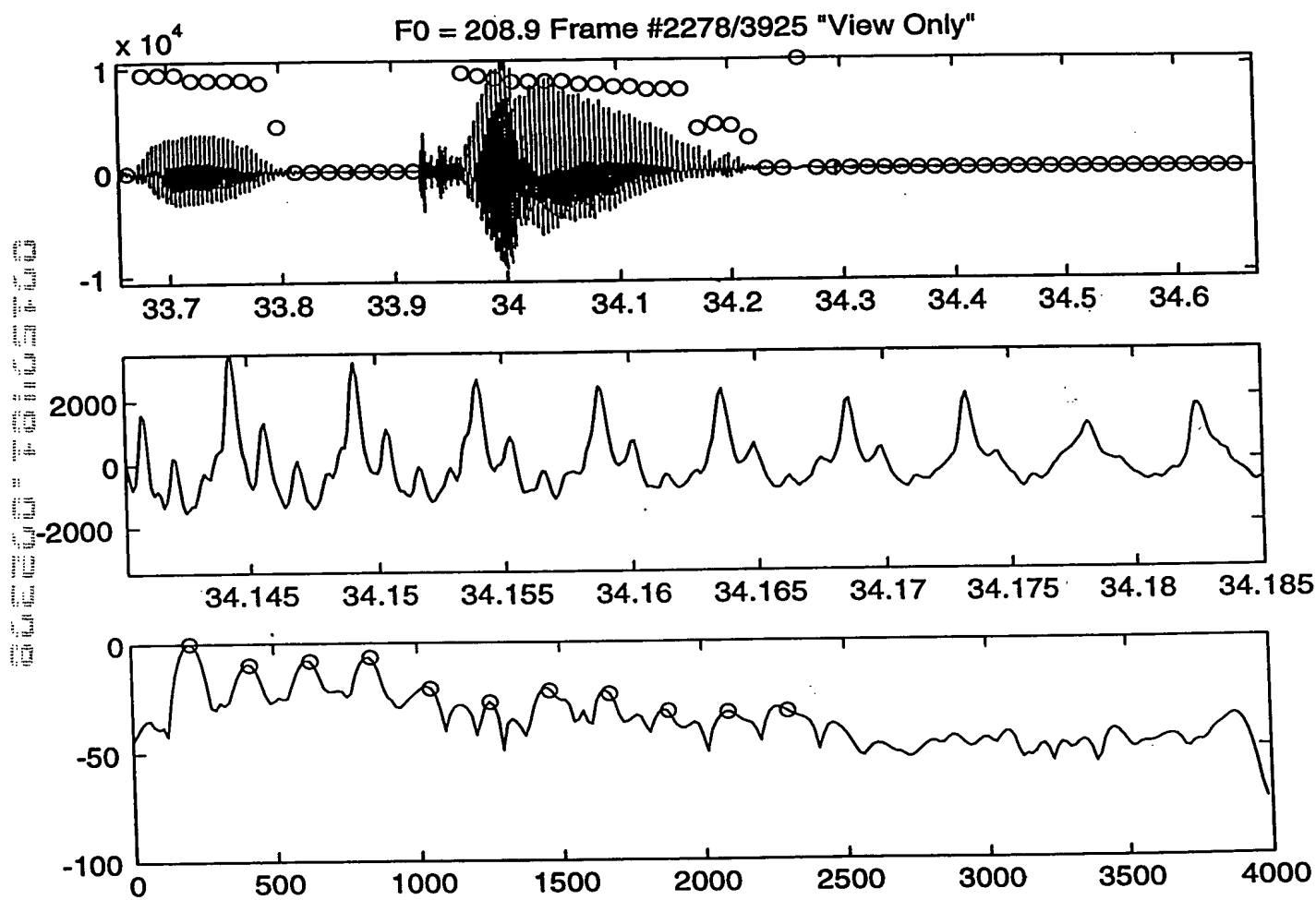
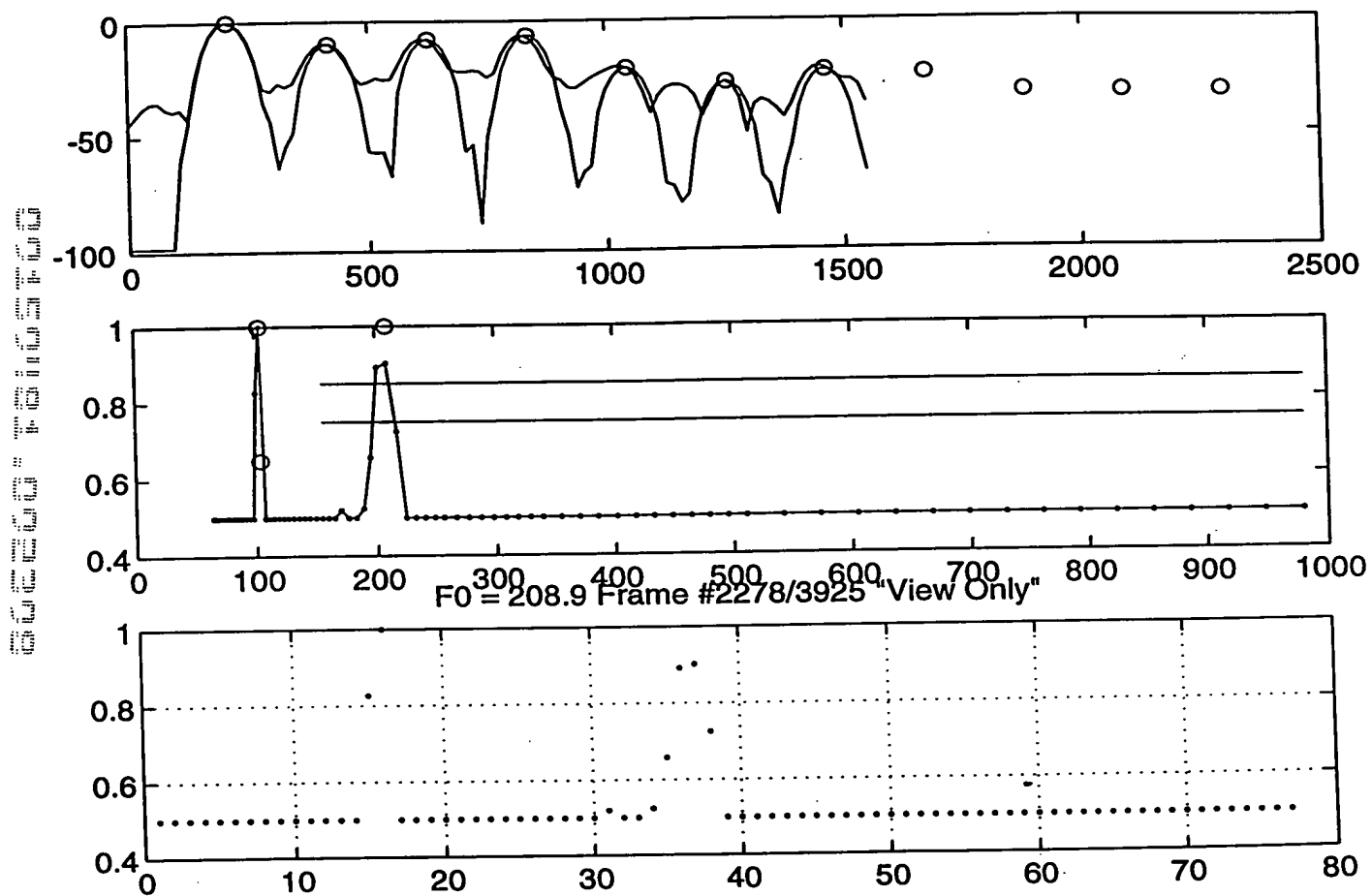


Fig. 9C



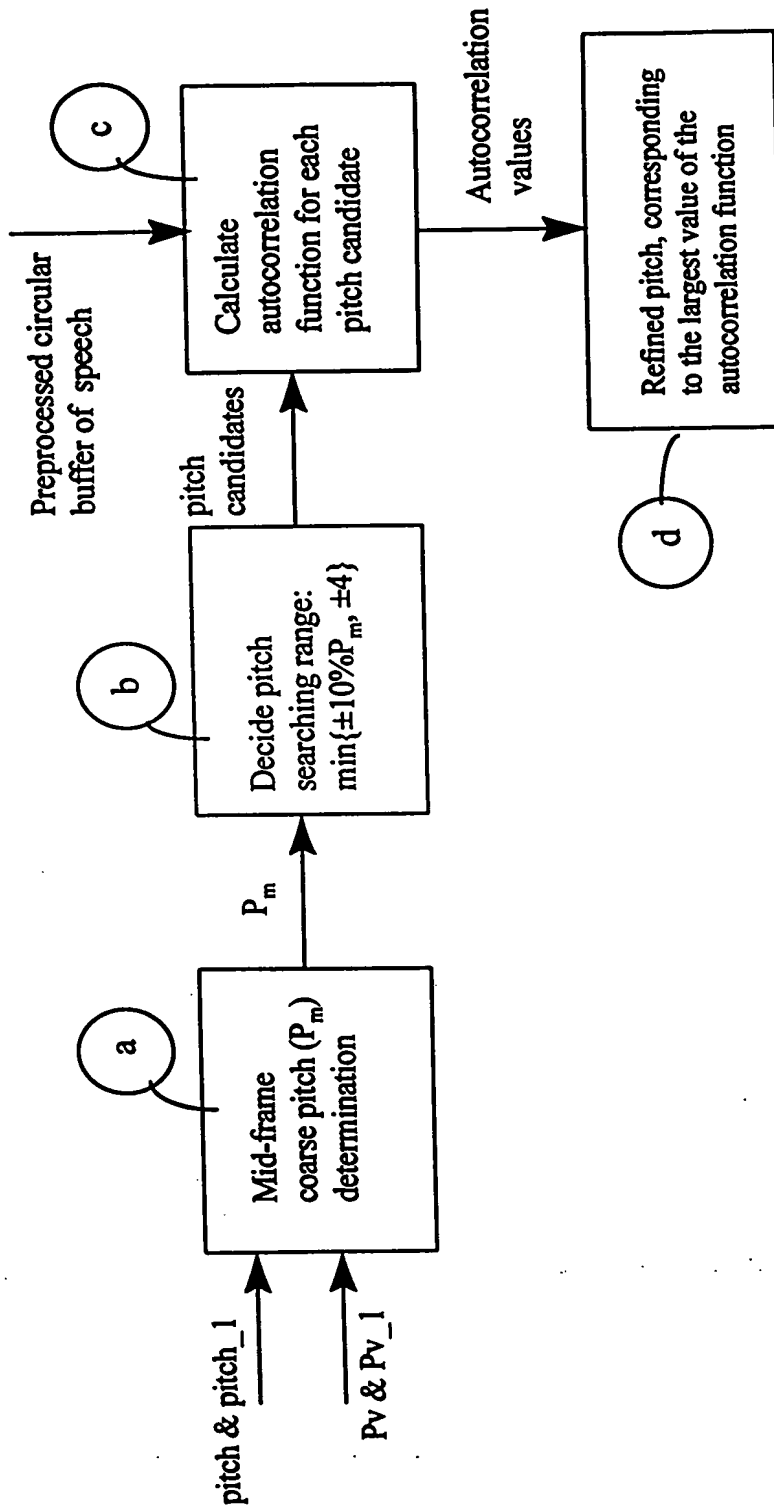


Fig. 10

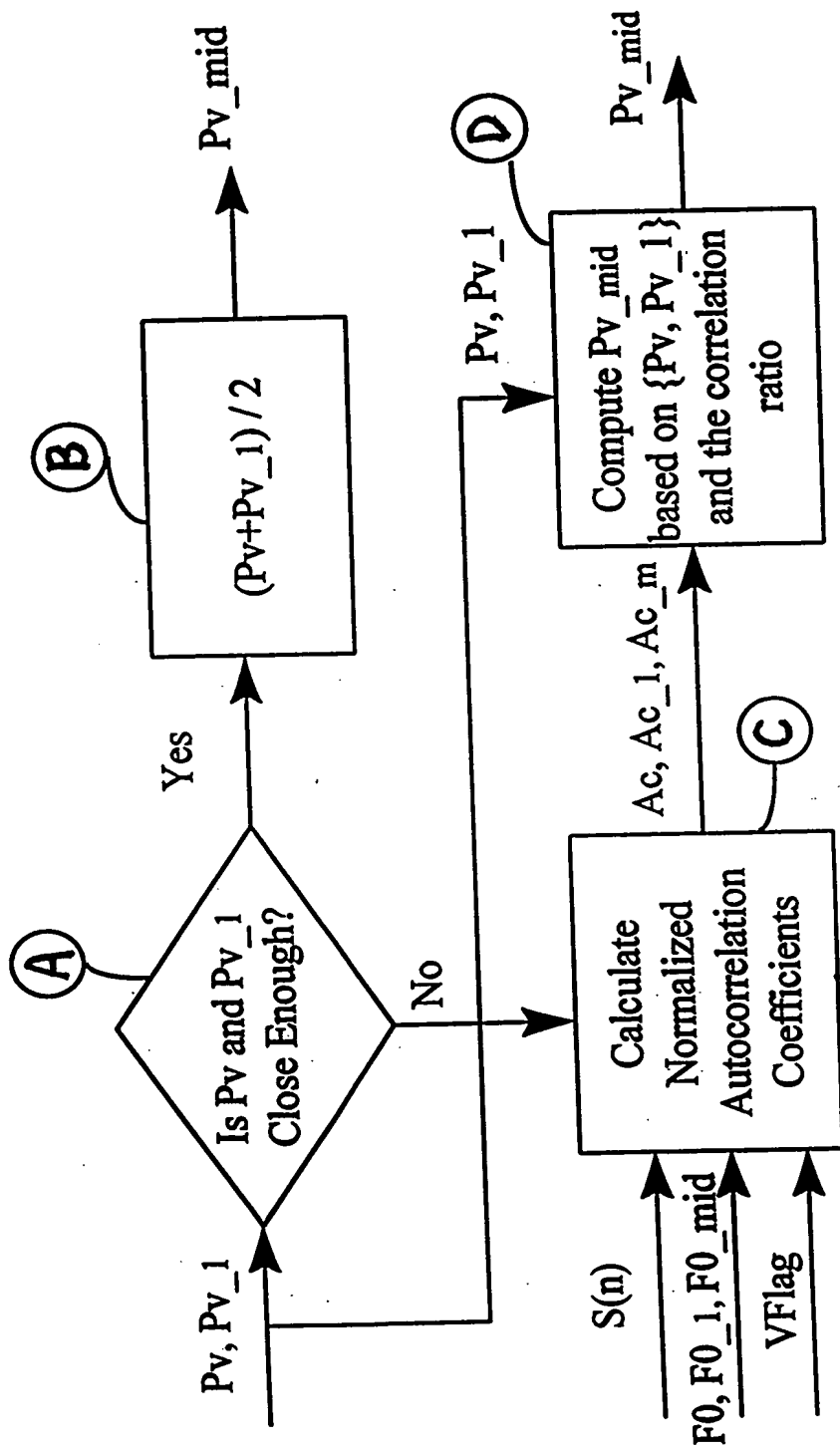


Fig. 11

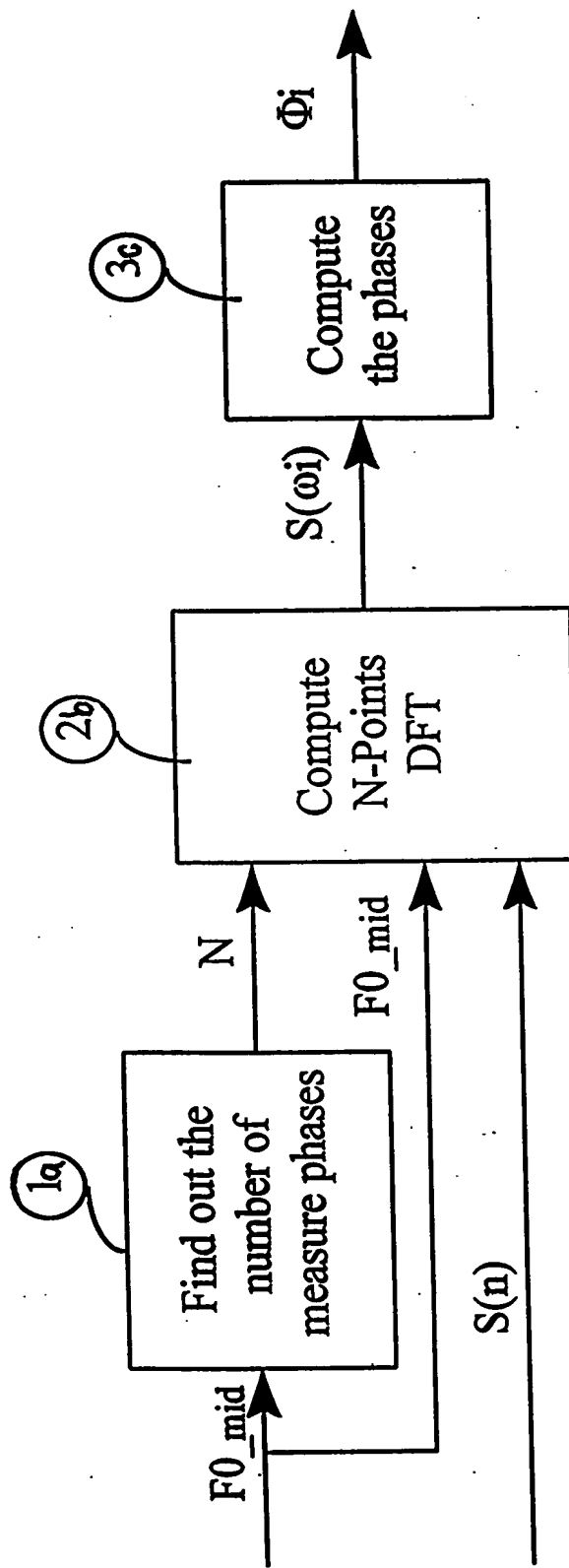


Fig. 12

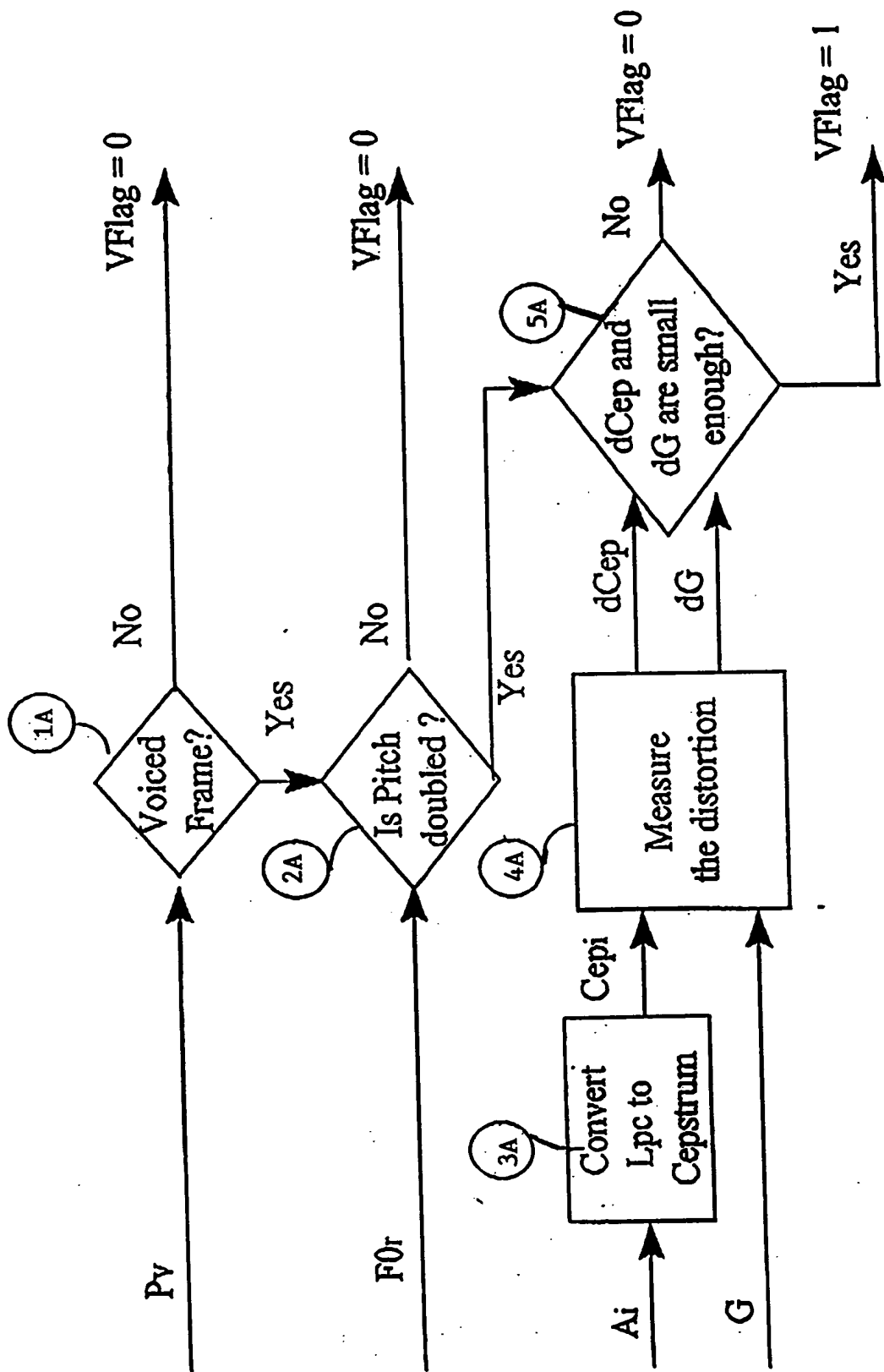


Fig. 13

Unnamed Plot

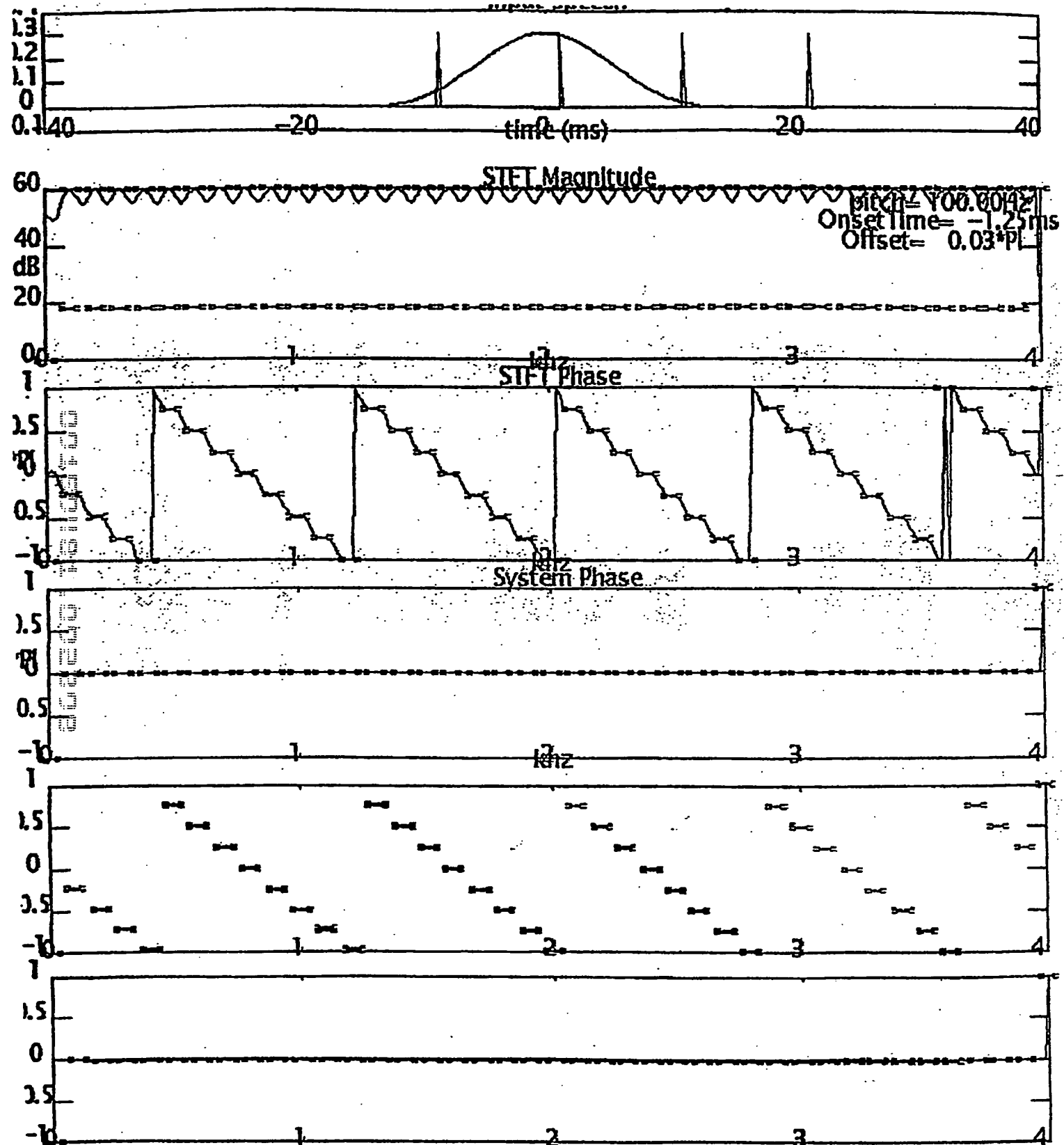
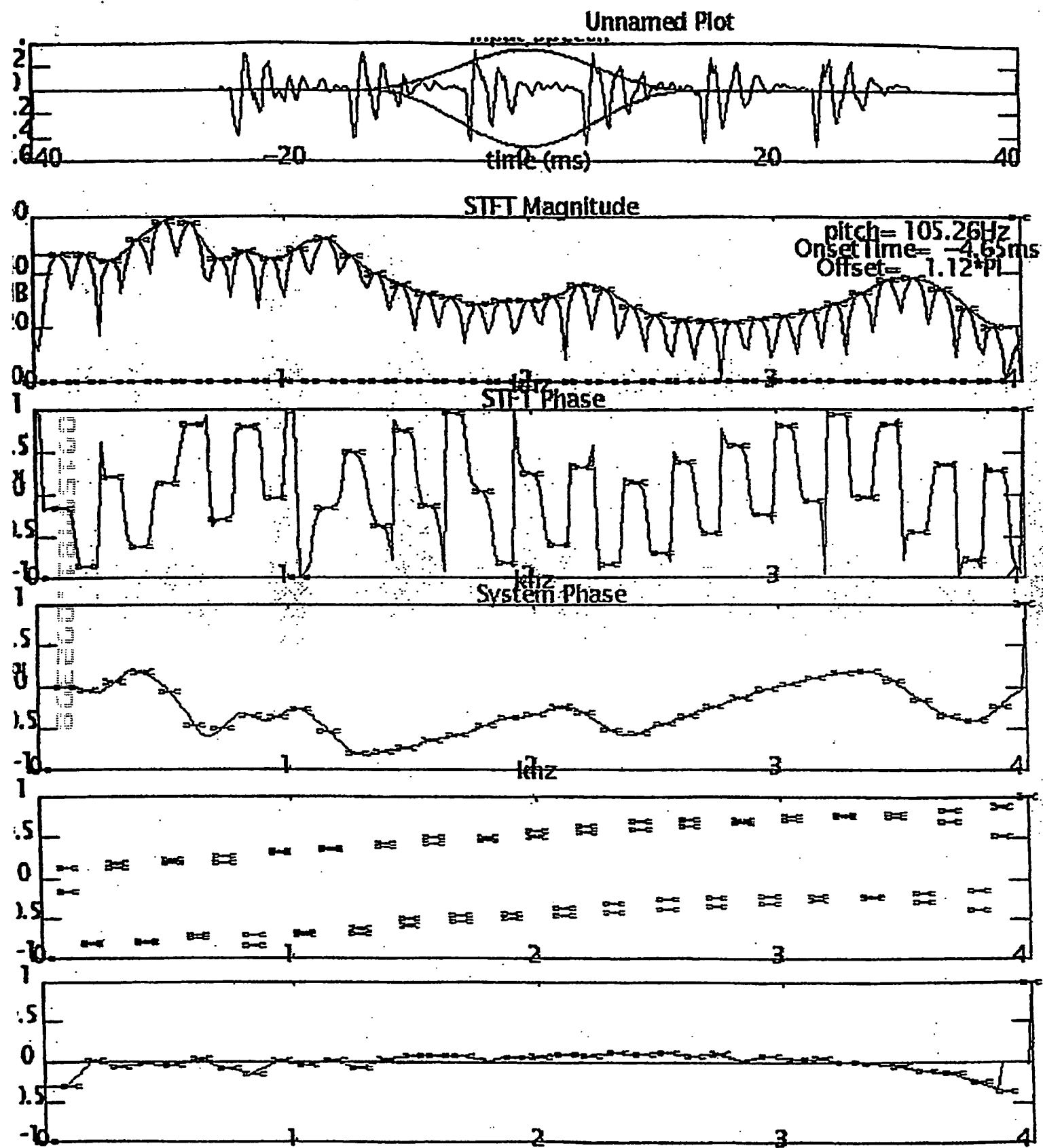
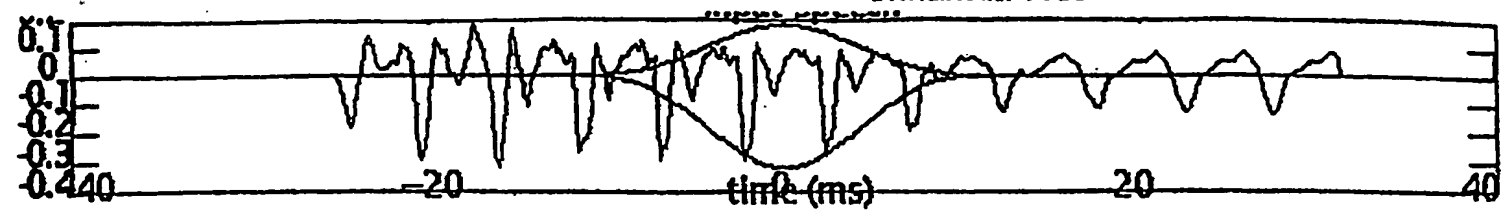


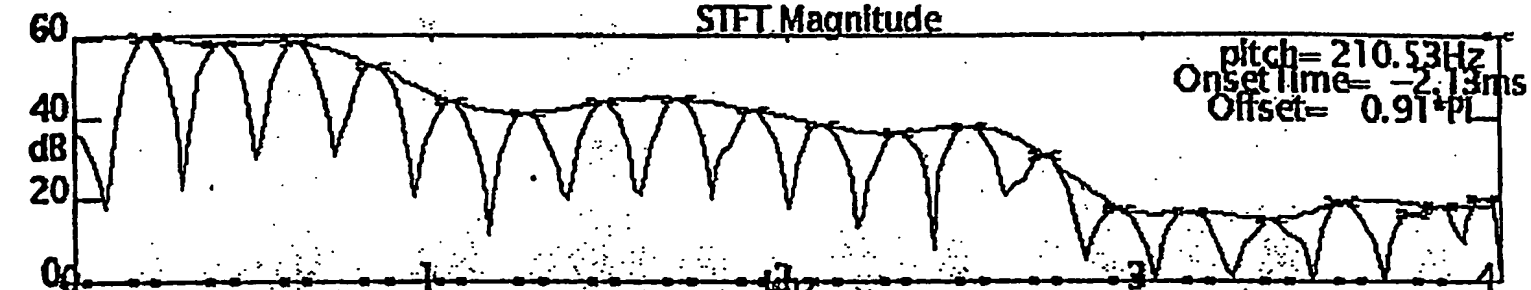
Fig. 15



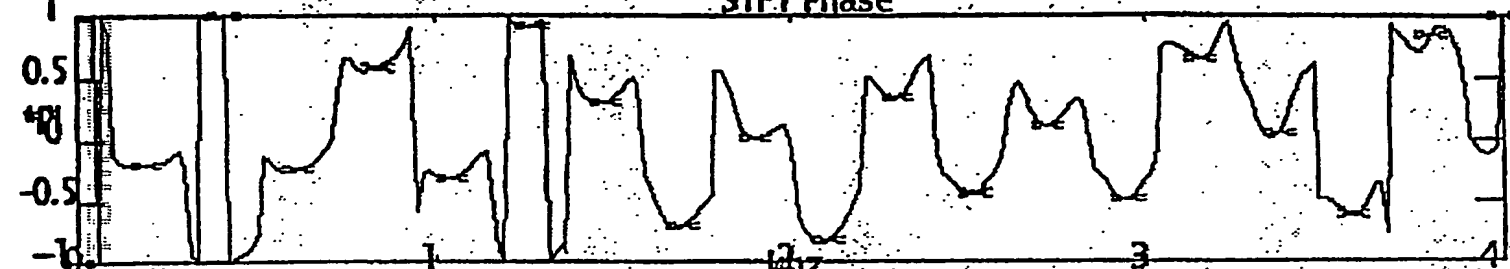
Unnamed Plot



STFT Magnitude



STFT Phase



System Phase

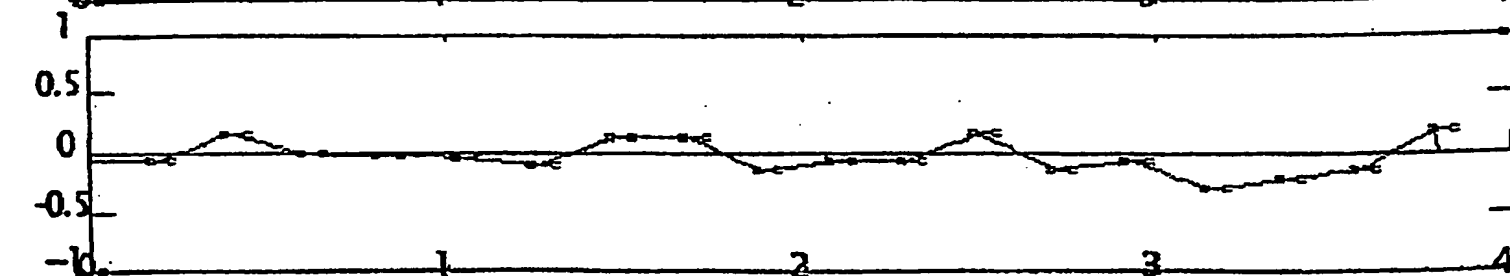
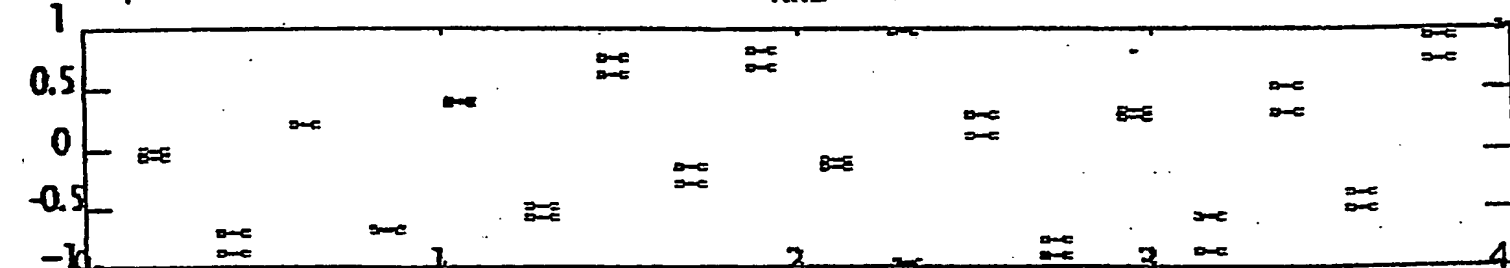
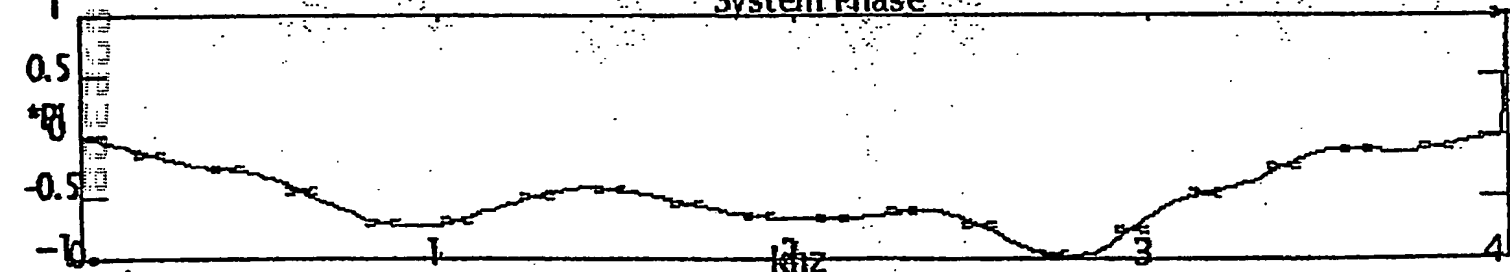


Fig. 17

Unnamed Plot

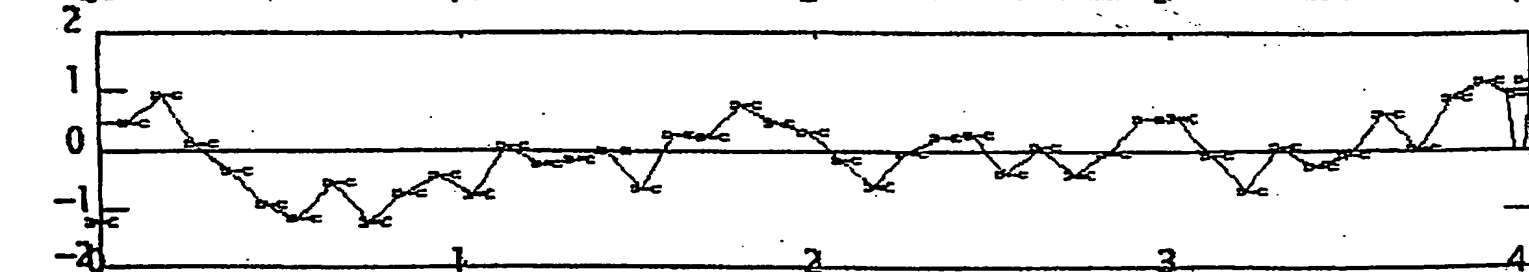
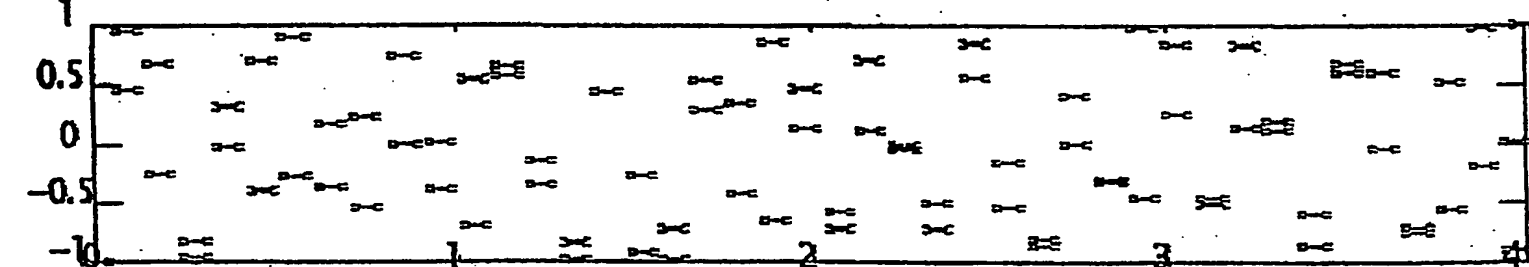
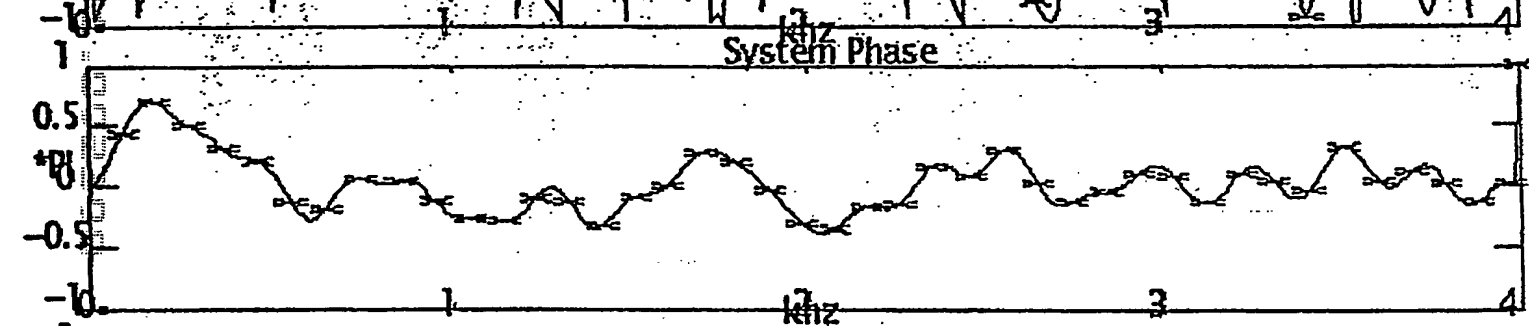
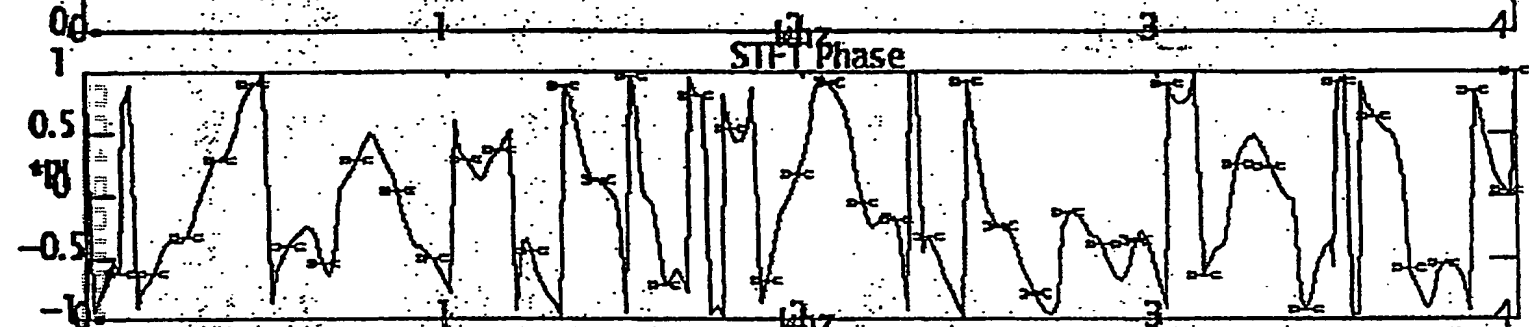
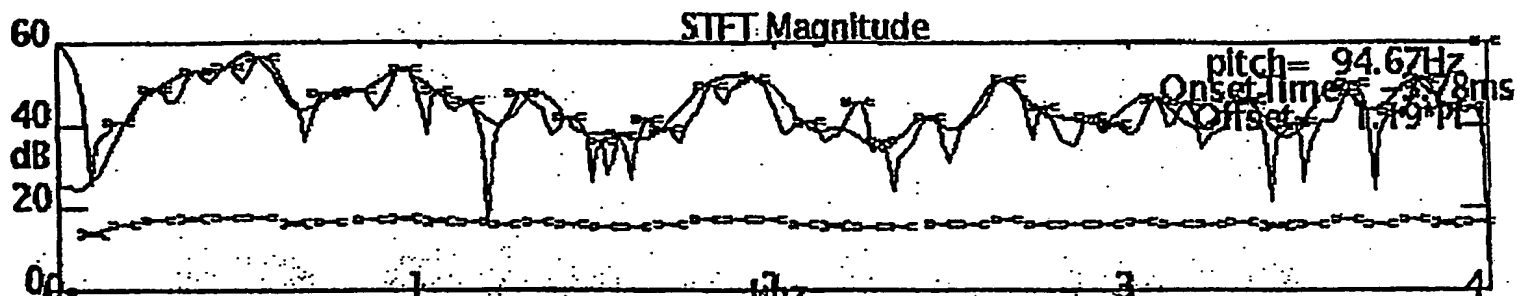
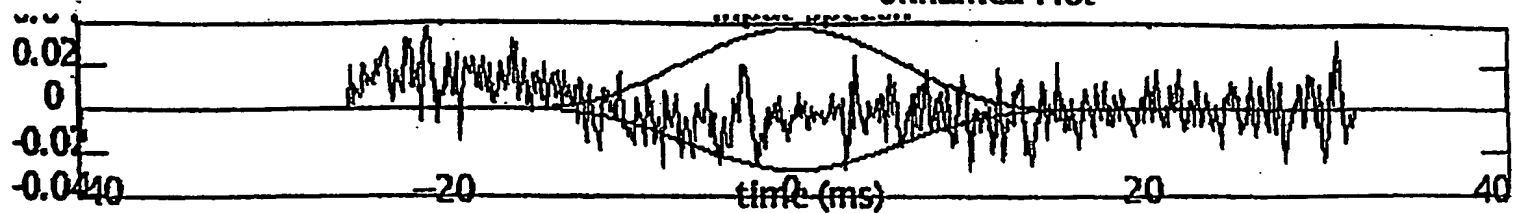
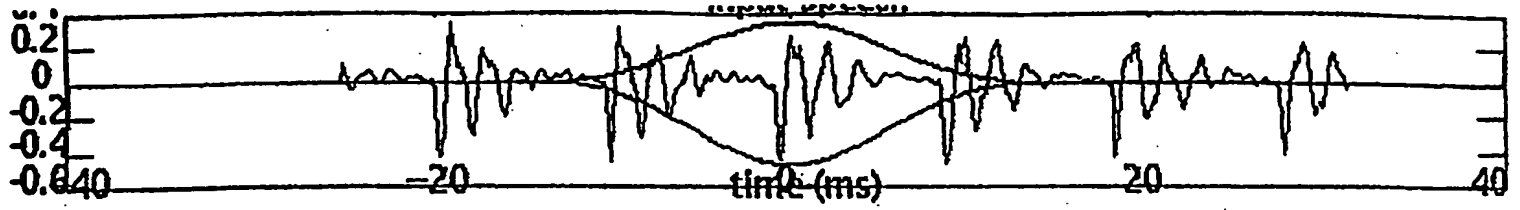
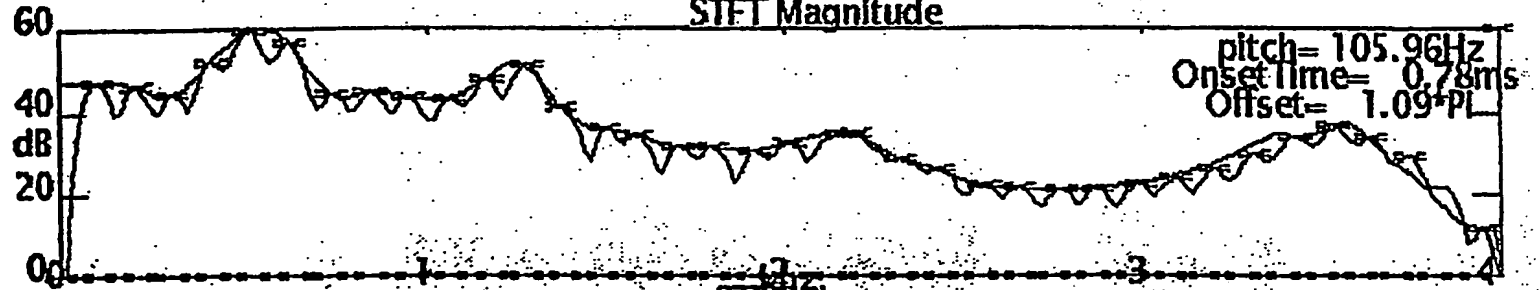


Fig. 18

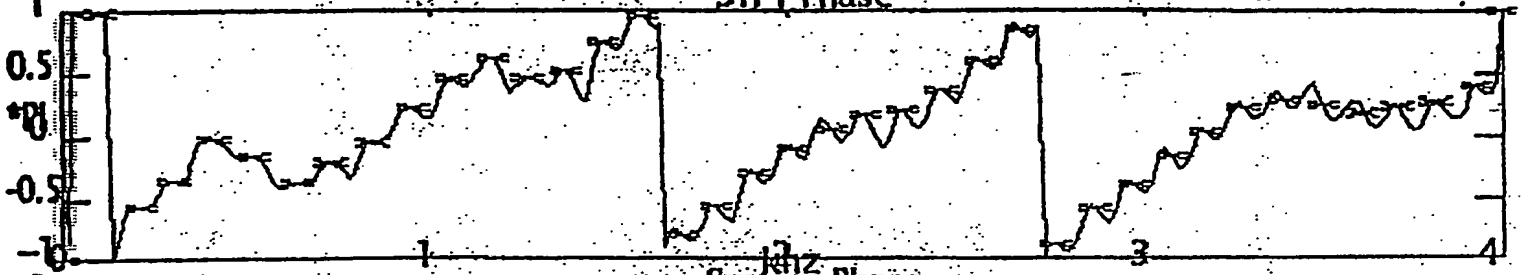
Unnamed Plot



STFT Magnitude



STFT Phase



System Phase

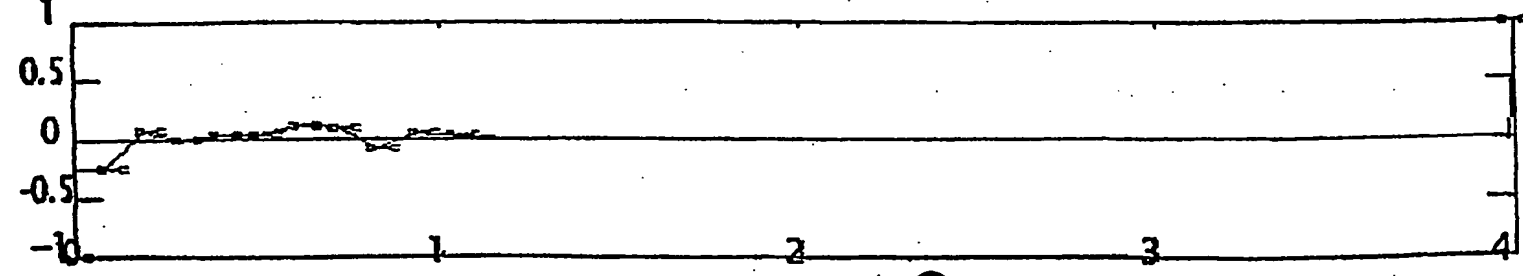
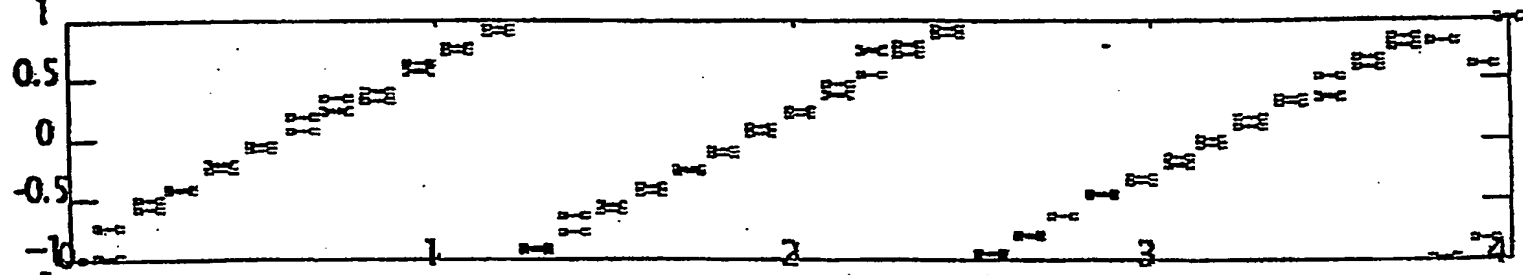
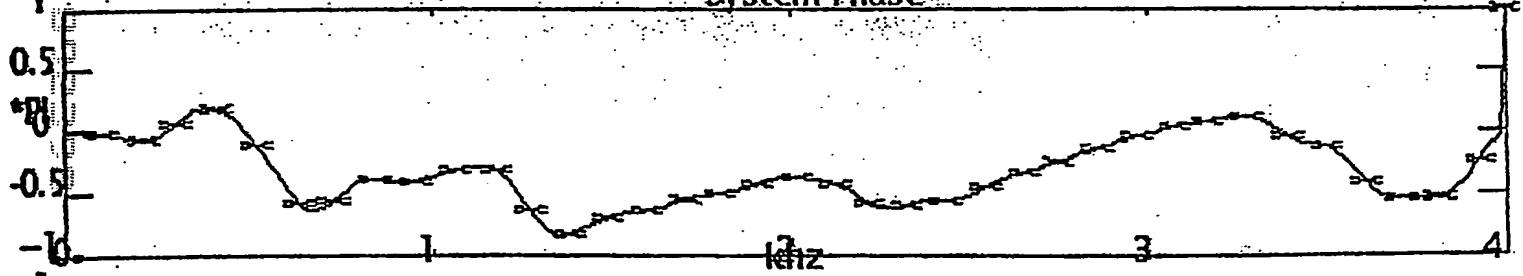


Fig. 19

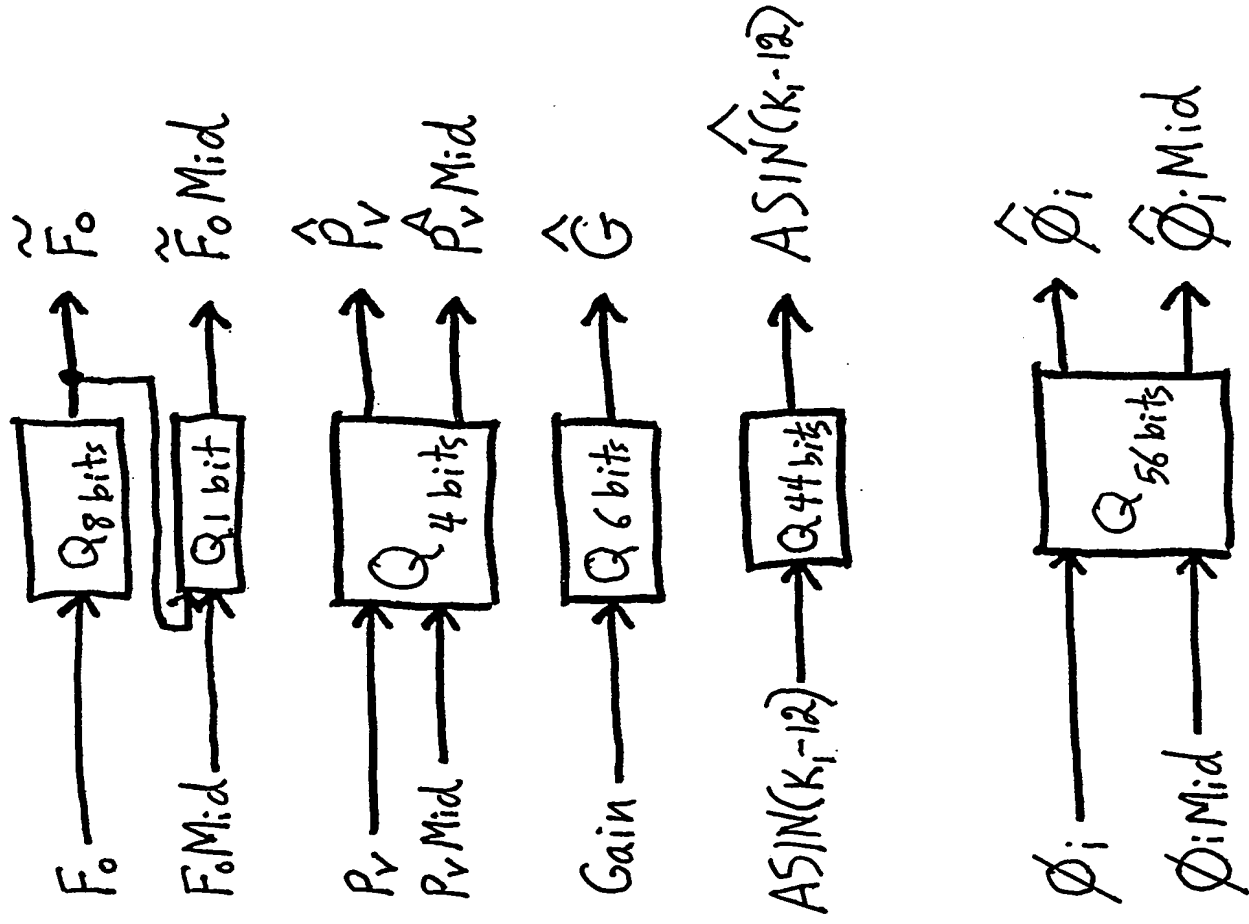


Fig. 20

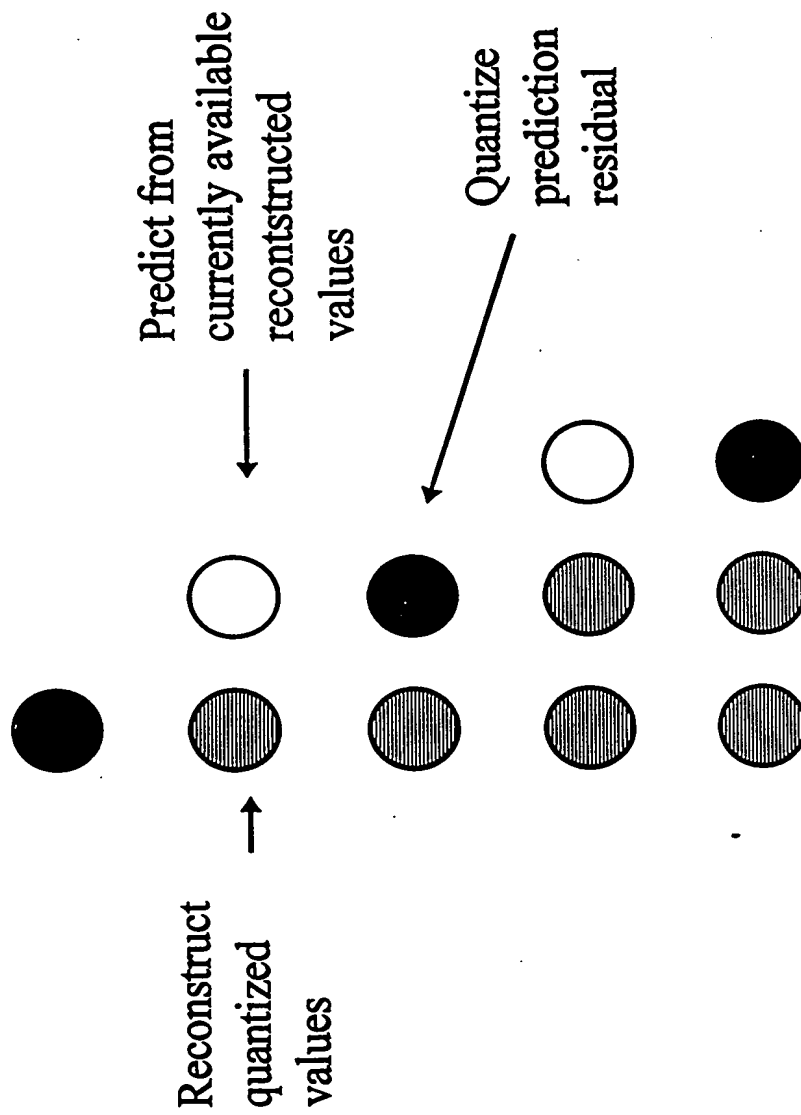


Fig. 21

Spectral Quantization



prediction of $AS(i)$

$$\hat{AS}(i) = \sum_{j=1}^{i-1} a_{ij} \tilde{AS}(j)$$

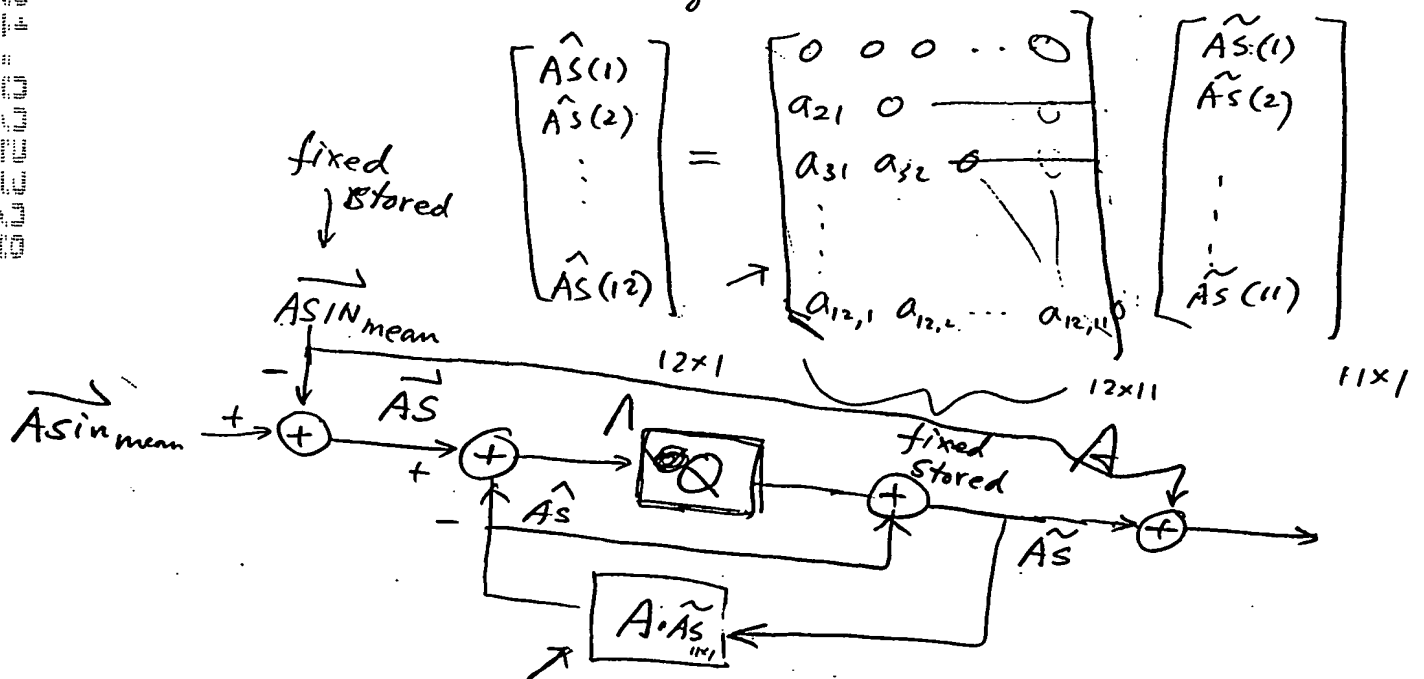


Fig. 21A

PHASE-PREDICTIVE CODING

$$\begin{array}{c}
 W_{-1} \text{---} W \\
 \hat{\Theta}_{-1} \text{---} \bar{\Theta} = \Theta_{-1} + \frac{W_{-1} + W}{2} \times T \\
 \cdot \Theta
 \end{array}$$

PHASE RESIDUAL = $\Theta - \bar{\Theta}$

W_{-1} = frequency at previous frame
 W = frequency at current frame
 Θ_{-1} = quantized phase at previous frame
 $\bar{\Theta}$ = predicted phase at current frame
 Θ = measured phase at current frame

Fig. 22A

SCATTER PLOT OF PREDICTION AND 20ms PHASE AND 10ms PHASE

20ms PHASE
ERROR



$(\theta_{20ms} - \theta_{10ms})$

K

$-\pi$

Fig. 22B

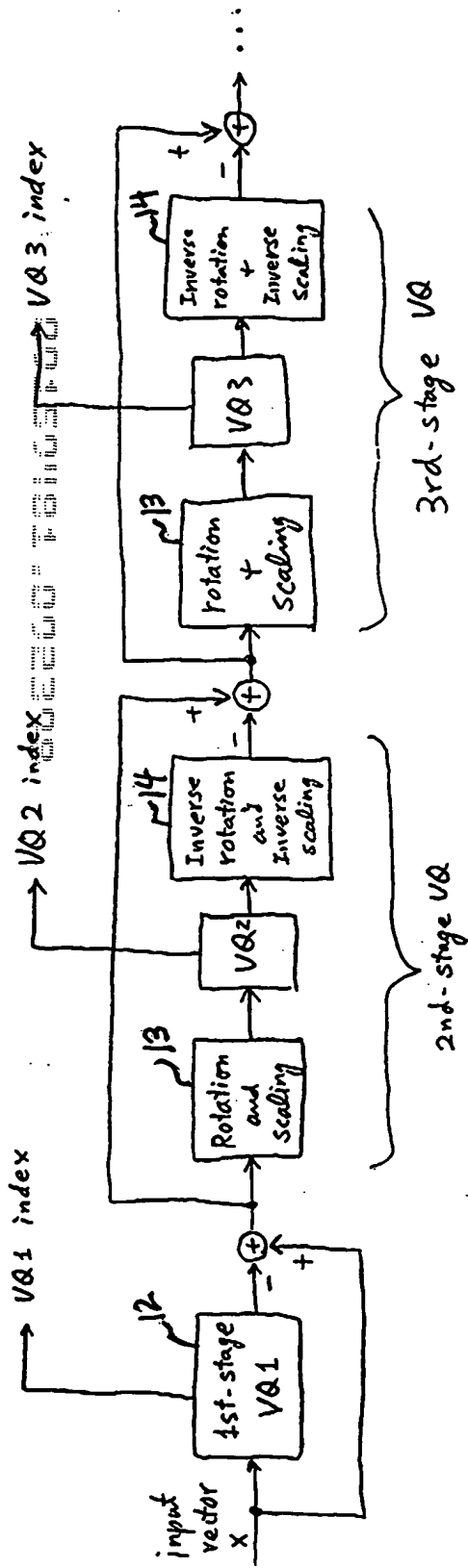


Fig. 23A

RS-MSVQ Encoder

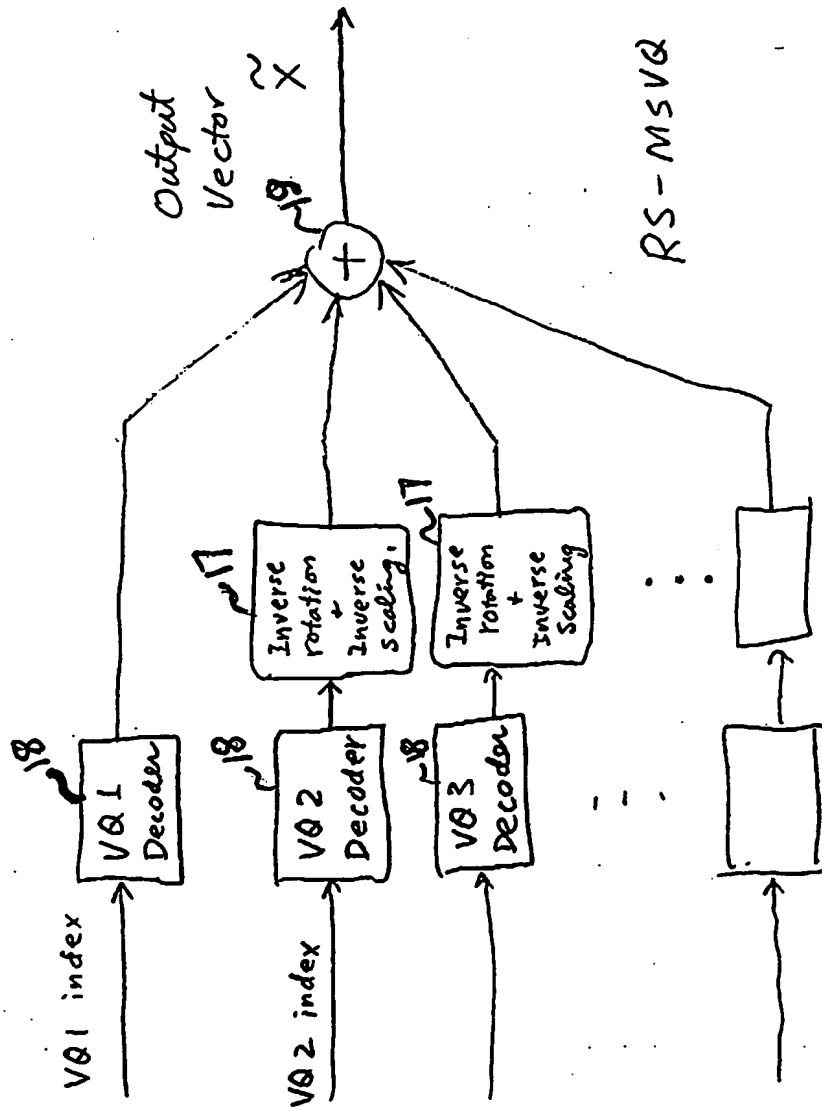
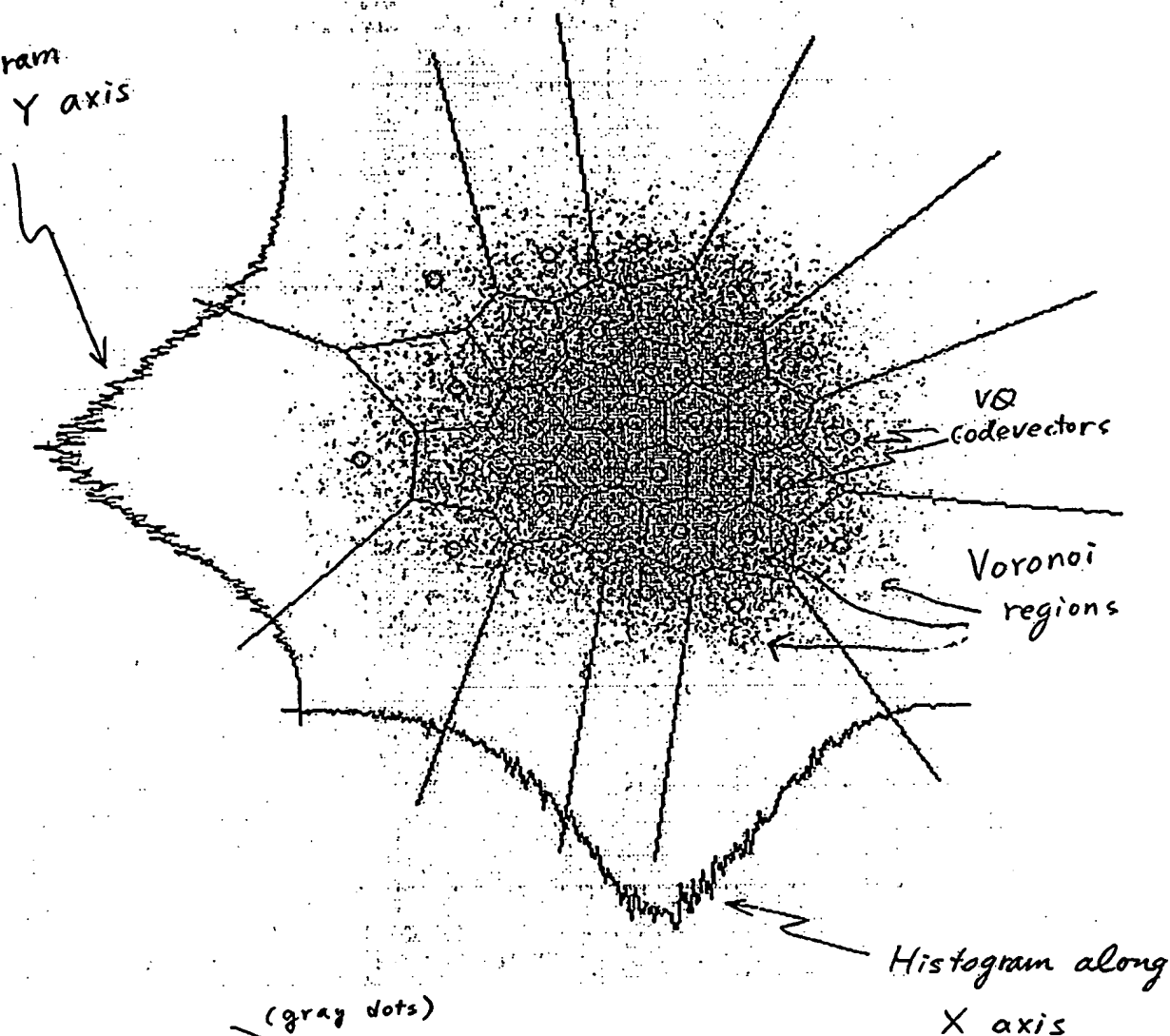


Fig. 23B

RS-MSVQ Decoder

SECRET

Histogram
along Y axis



Scatter plot (gray dots) of 4th pair of $ASIN(k)$ intra-frame prediction error, the histogram along each direction, and the corresponding 1st-stage 5-bit VQ codebook and Voronoi regions

Fig. 24A

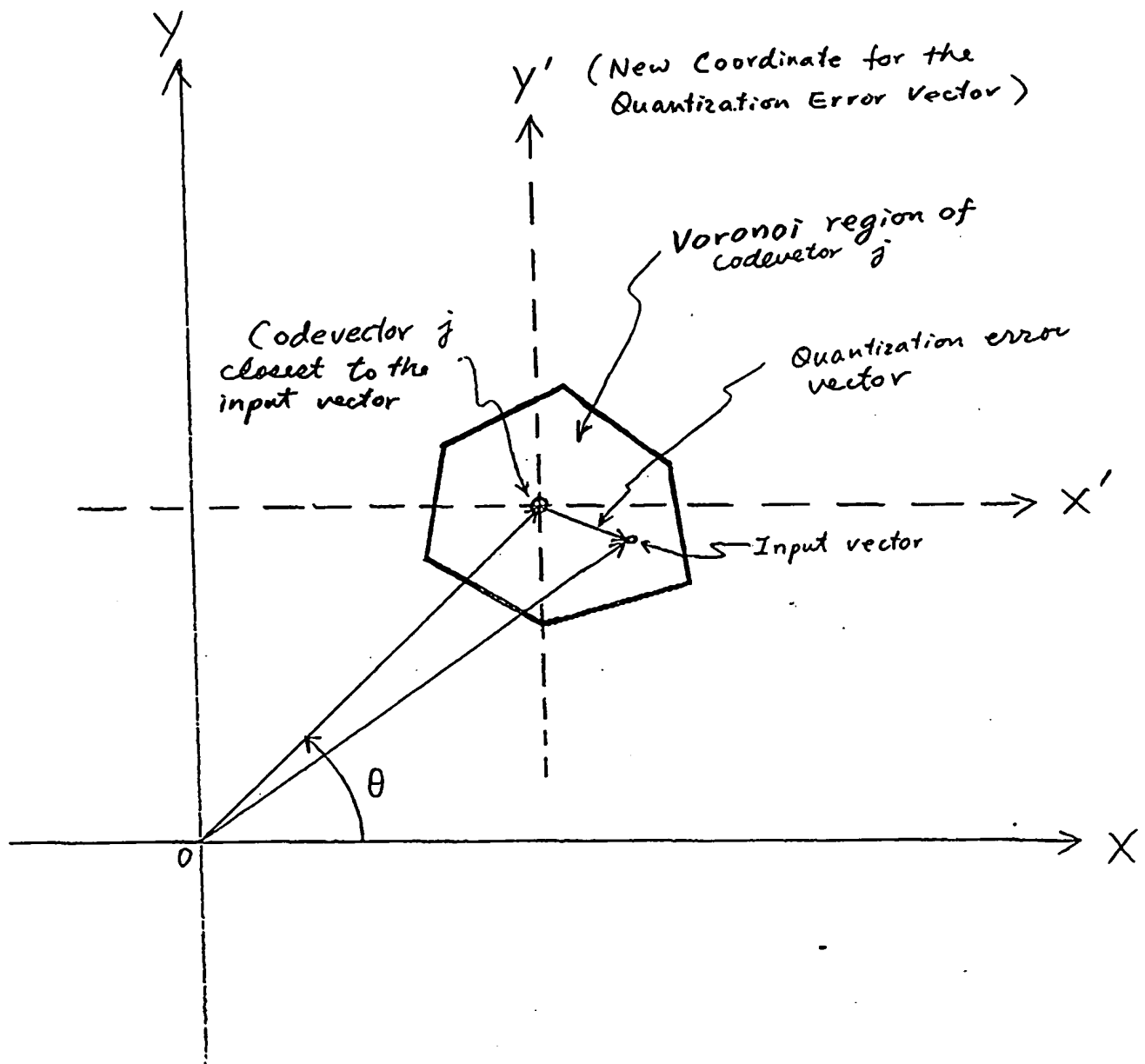


Fig. 24 B Illustration of the effect of subtracting the closest codevector for the input vector to get the quantization error vector.

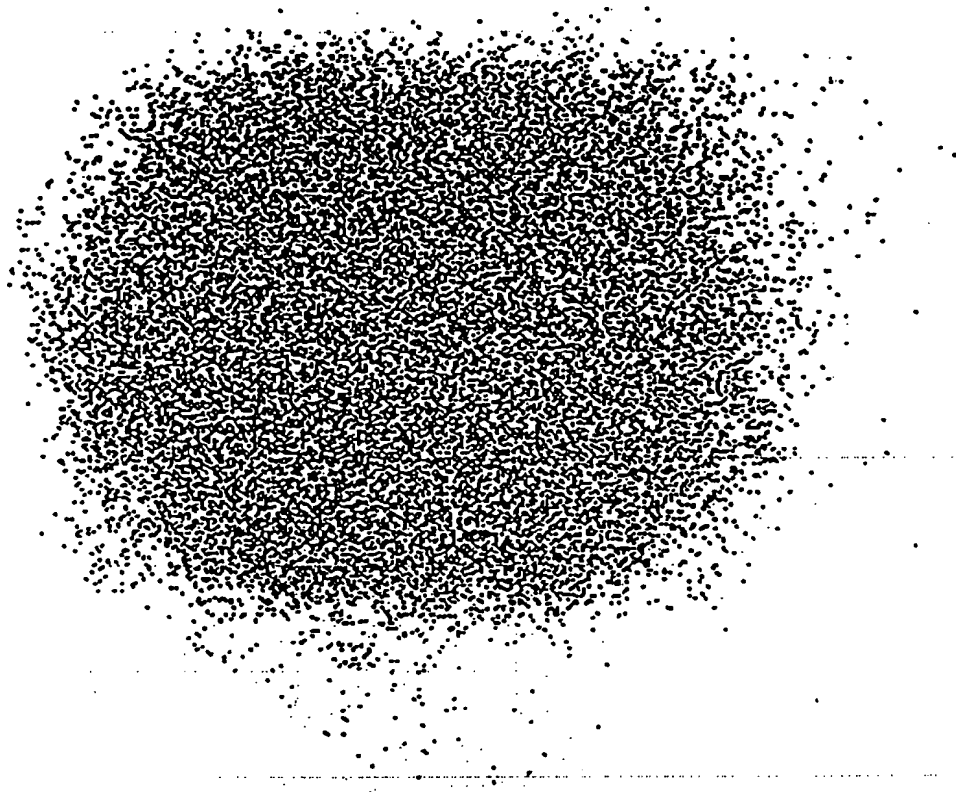
Fig. 24B

A black and white photograph of a biological specimen, likely a plant stem or root, showing a network of dark, branching lines (possibly vascular bundles or roots) against a lighter, textured background. Several small, dark, circular spots are visible along the main axis and branches.

Fig. 24C

A large, dense, circular cluster of black dots, resembling a stylized letter 'A' or a dense collection of points, centered on a white background. The dots are tightly packed in the center and become more sparse towards the edges, forming a roughly circular shape. The overall appearance is that of a high-contrast, black-and-white image, possibly a scan of a physical object or a digital graphic.

Fig. 25

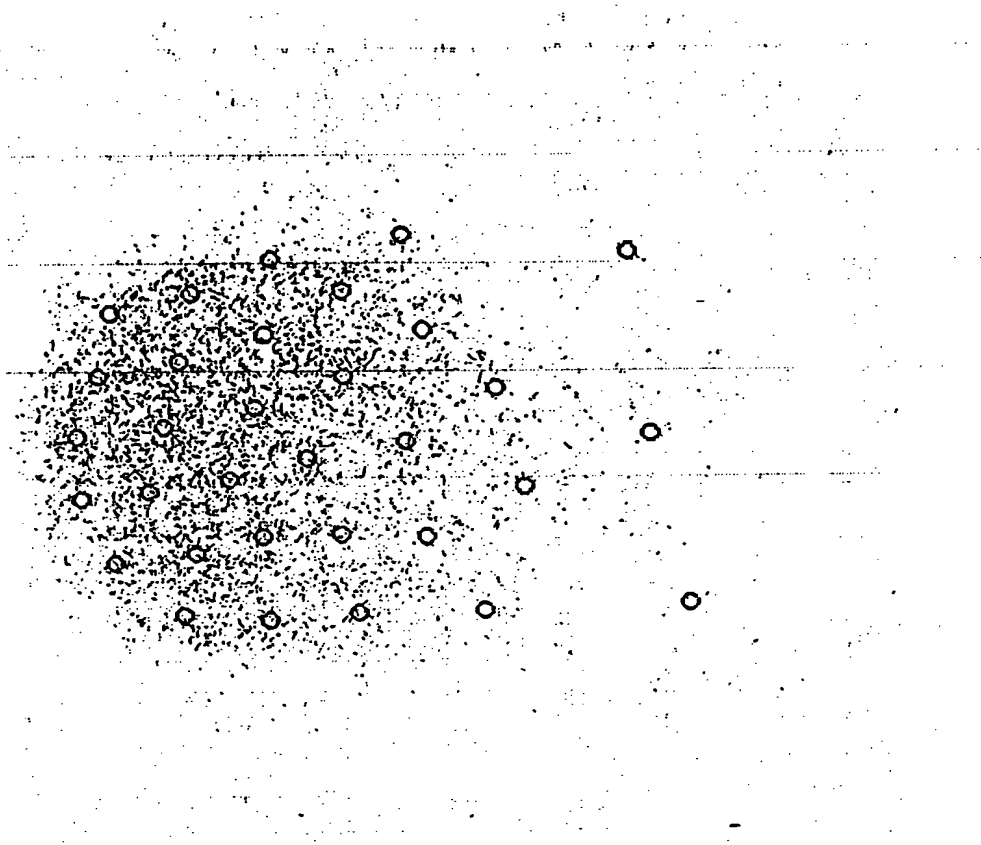


With hand-tuned rotation angles
 — inner cells of 1st pair of $ASIN(k)$
 of 1st-stage VQ of

Fig. 26

A complex, dense, and irregular pattern of black lines and dots, resembling a heavily textured or noisy image, possibly a corrupted scan or a highly detailed abstract drawing. The pattern is centered and fills most of the frame, with some lines extending towards the edges. The overall appearance is that of a high-contrast, black-and-white image with significant visual noise and a lack of clear geometric structure.

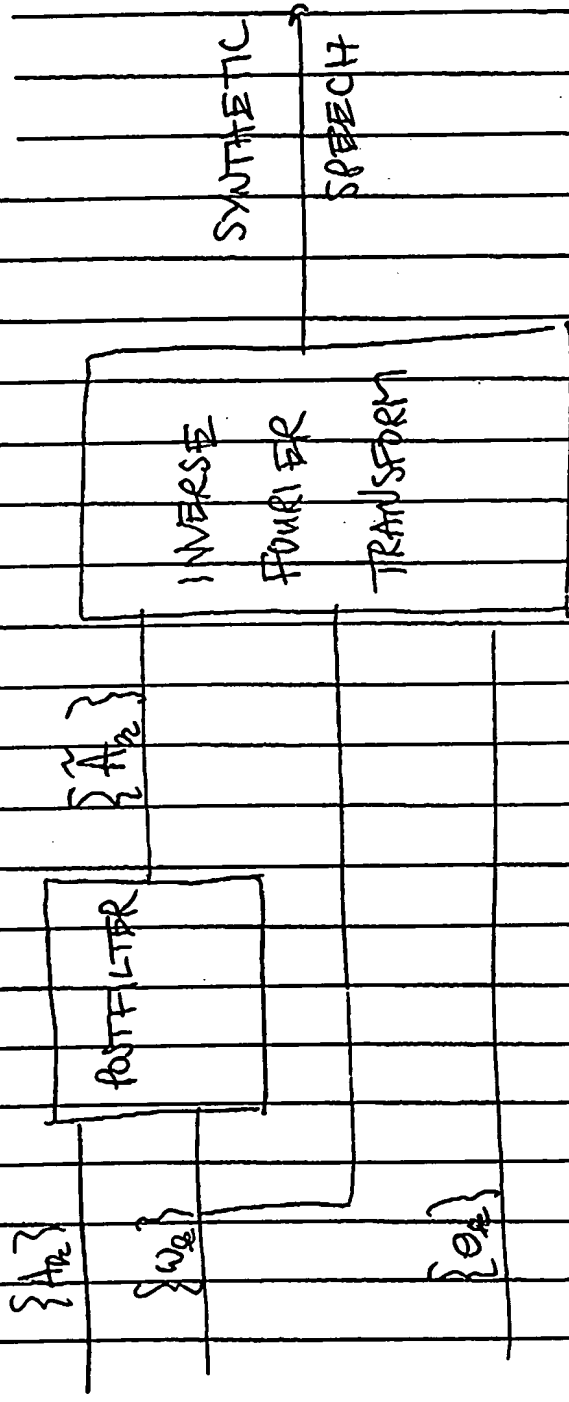
Fig. 27



Outer-cell 1st-stage VQ error vector distribution
and corresponding 2nd-stage VQ codebook (small circles)
for 1st pair of $ASIN(k)$

Fig. 28

SINUSOIDAL SPEECH SYNTHESIS



$i_{th} = k^{th}$ sine-wave amplitude
 $\omega_k = k^{th}$ sine-wave frequency
 $\phi_k = k^{th}$ sine-wave phase
 $\hat{A}_{n_k} = k^{th}$ post-filtered sine-wave amplitude

Fig. 29

CANONICAL FREQUENCY-DOMAIN POSTFILTER

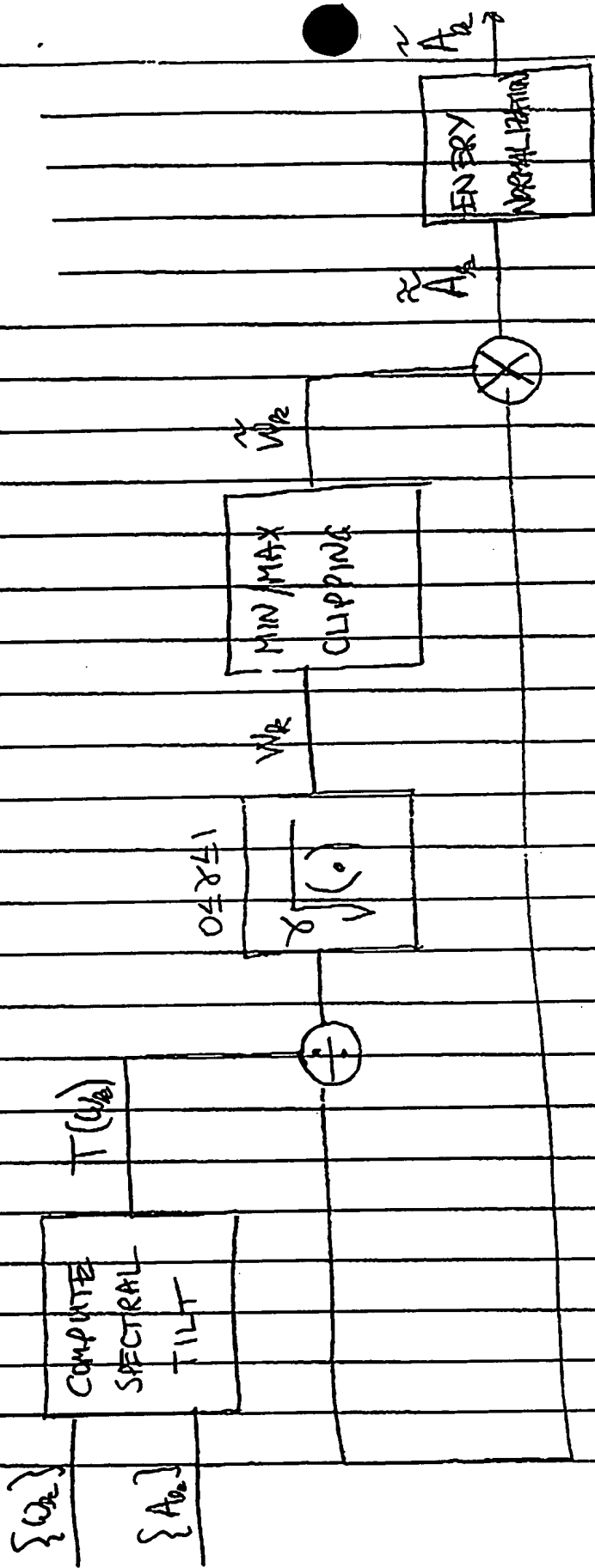
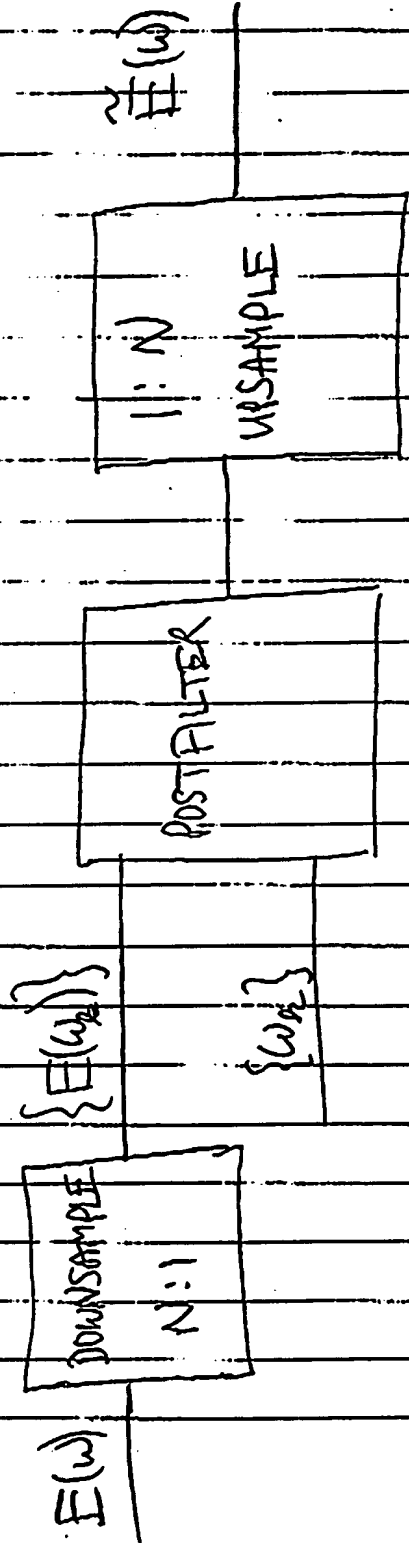


Fig. 30

CONSTANT COMPLEXITY POSTFILTER



$E(w)$ = amplitude envelope

w_k = downsampled frequencies

$\tilde{E}(w)$ = post-filtered amplitude envelope

Fig. 31

CONSTANT COMPLEXITY POSTFILTER COMPUTED

FROM CEPSTRAL COEFFICIENTS

$$\{C_m\}$$

CEPSTRAL COEFFICIENTS
TO AMPLITUDE ENVELOPE

$$E(\omega)$$

CONSTANT
COMPLEXITY
POST FILTER

$$\hat{E}(\omega)$$

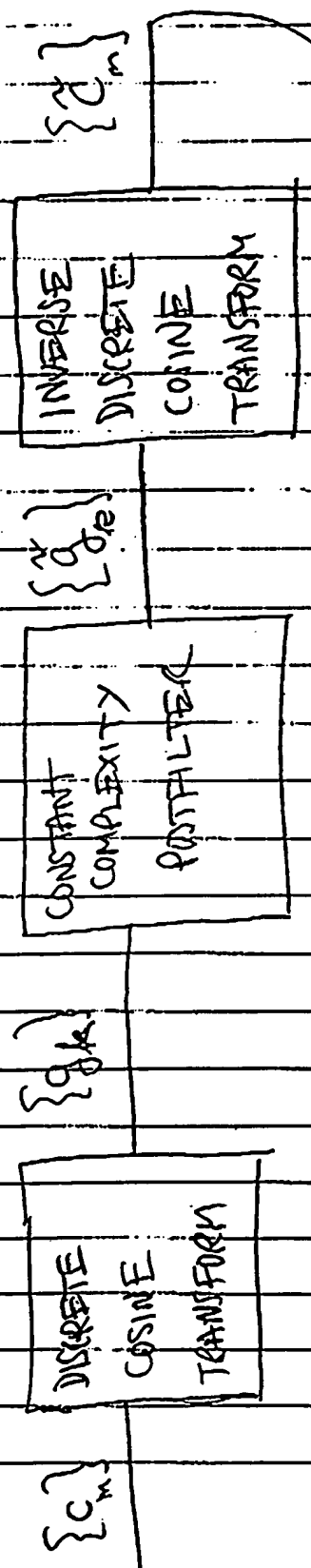
$$C_m = \frac{1}{m} \text{ CEPSTRAL COEFFICIENT}$$

$$E(\omega) = \text{AMPLITUDE ENVELOPE}$$

$$\hat{E}(\omega) = \text{POST-FILTERED AMPLITUDE ENVELOPE}$$

Fig. 32

FAST CONSTANT COMPLEXITY POSTFILTER



CENTRAL COEFFICIENTS
TO
AMPLITUDE ENVELOPE

$\hat{E}(u)$

Fig. 33

$c_m = m^{th}$ cepstral coefficient
 $g_k = k^{th}$ DCT coefficient = k^{th} channel gain
 $\tilde{g}_k = k^{th}$ post-filtered channel gain
 $\tilde{c}_m = m^{th}$ post-filtered cepstral coefficient
 $\hat{E}(u) =$ post-filtered amplitude envelope

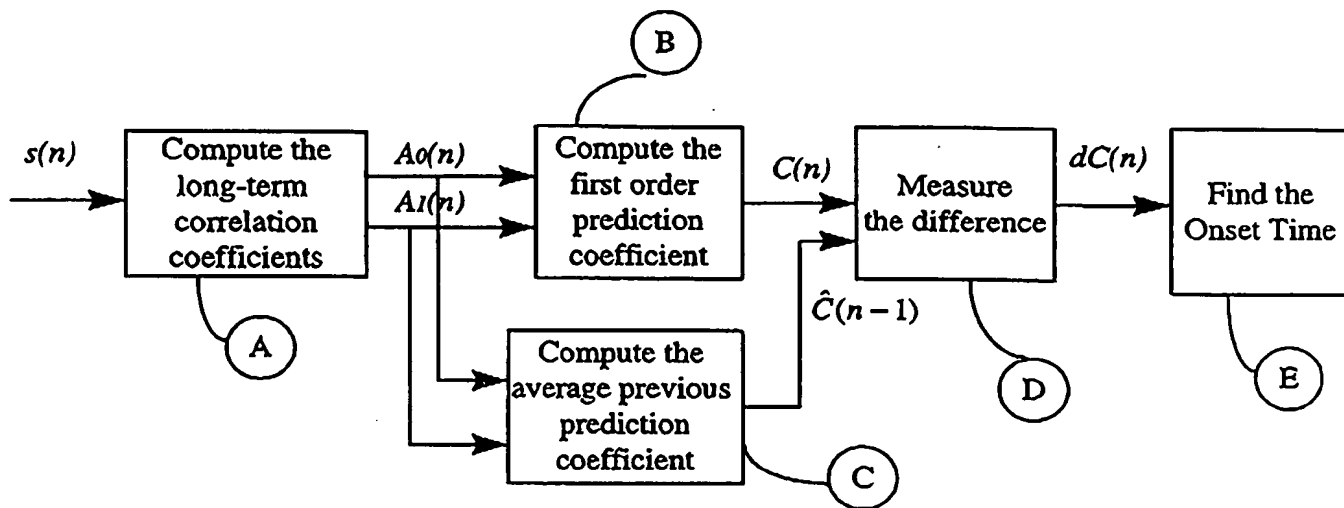


Figure 34.

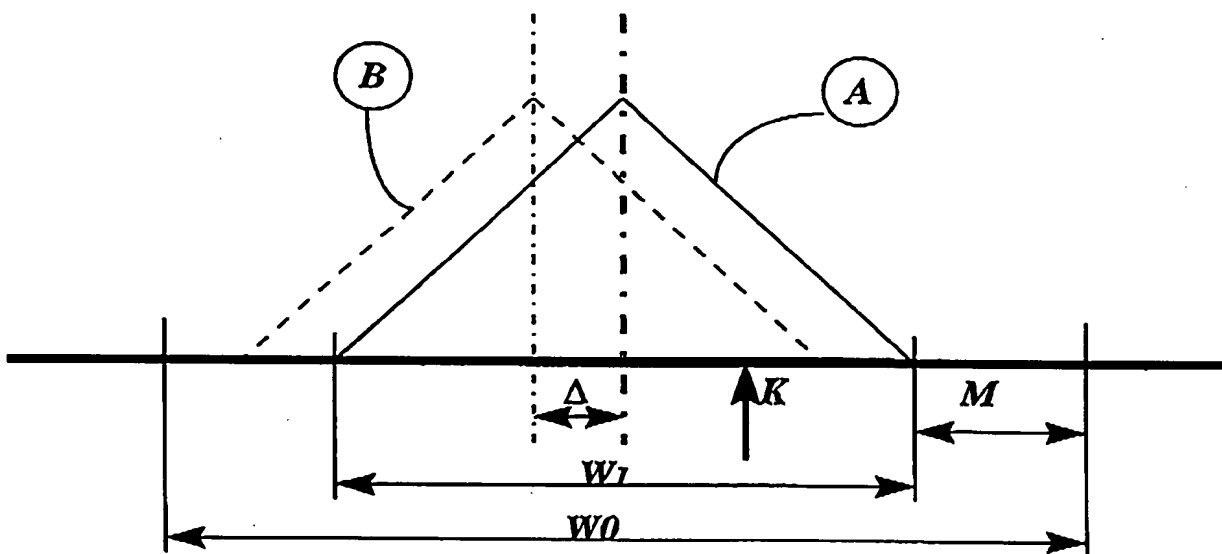


Figure 35.